EFFECTS OF IMAGE COMPRESSION ON DATA INTERPRETATION FOR TELEPATHOLOGY

A Dissertation
Presented to
The Academic Faculty

by

Saunya Michelle Williams

In Partial Fulfillment of the
Requirements for the Degree
Doctor of Philosophy in the
School of Electrical and Computer Engineering

Georgia Institute of Technology
December 2011

EFFECTS OF IMAGE COMPRESSION ON DATA INTERPRETATION FOR TELEPATHOLOGY

Approved by:

Dr. Nikil S. Jayant, Advisor
School of Electrical and Computer Engineering
Georgia Institute of Technology

Dr. Gee-Kung Chang
School of Electrical and Computer Engineering
Georgia Institute of Technology

Dr. Arthur Koblasz
School of Electrical and Computer Engineering
Georgia Institute of Technology

Dr. Gregory D. Abowd
School of Interactive Computing
Georgia Institute of Technology

Dr. Mark L. Braunstein
School of Interactive Computing
Georgia Institute of Technology

Date Approved: August 25, 2011

DEDICATION

[22]Through the LORD's mercies we are not consumed because His compassions fail not. [23]They are new every morning; great is Your faithfulness. [24]"The LORD is my portion," says my soul, "Therefore I hope in Him!" [25]The LORD is good to those who wait for Him, to the soul who seeks Him.

Lamentations 3:22-25 (King James Version)

To my mother (Linda), your immeasurable and selfless sacrifices have allowed me to become the woman that I am today. To all of my grandmothers that are resting in heaven (Ida, Anna, Ethel, and Olivia), your resilient and triumphant spirit continues to fuel my soul. Thank you all for being a beacon in my life.
I dedicate this dissertation to each of you.

ACKNOWLEDGEMENTS

With the unparalleled grace of *GOD*, I have been able to produce this dissertation and to complete my journey to a doctorate degree. I am truly humbled and absolutely blessed to have such an amazing testimony. Additionally, I would like to extend my sincere gratitude to the numerous individuals that also helped me during this pursuit.

To Georgia Institute of Technology (Georgia Tech) and the School of Electrical and Computer Engineering (ECE), I am so grateful for the highly-coveted opportunity to pursue my dream. For providing me with financial support and many wonderful experiences, I give enormous gratitude to the following: School of ECE, Facilitating Academic Careers in Engineering and Science (FACES), IBM, FOCUS, National Consortium for Graduate Degrees for Minorities in Engineering and Science, Inc. (GEM), Office of Minority Educational Development (OMED), Student and Teacher Enhancement Partnership (STEP), and Center for the Enhancement of Teaching and Learning (CETL).

Dr. Nikil S. Jayant, the best advisor on the planet, has been beyond instrumental in helping me to earn my doctorate. He has provided me with invaluable insight and unconditional support. During some of my most difficult times, Dr. Jayant has been an inspiration and helped me to overcome my challenges. I had the freedom to explore, to learn, and to surpass what I once thought was impossible…thank you Dr. Jayant!! Also, I give many thanks to Dr. Alexis B. Carter at Emory University for the "crash course" in pathology and abundant assistance during the infancy of my research. For the collaboration and opportunity to extend my research, I must thank everyone at the Center

for Comprehensive Informatics at Emory University. In addition, I am truly grateful to Dr. Gee-Kung Chang, Dr. Gregory D. Abowd, Dr. Arthur Koblasz, and Dr. Mark L. Braunstein for serving on my dissertation committee.

While an undergraduate student at North Carolina A&T State University (A&T), Dr. Eric A. Cheek taught my course on circuit analysis. I thank Dr. Cheek for being a consistent role model and pillar in my life while I took a few detours along the way to Ph.D. As a graduating senior at A&T, I had the pleasure of meeting Dr. Calvin Mackie and was captivated by his triumphant story. I truly appreciate both Dr. Cheek and Dr. Mackie for helping me to view academia through a different lens.

I am extremely thankful for the friendship of Dr. Cherita L. Corbett and Dr. Raheem A. Beyah that has extended over many years. I remember questioning my decision to become a doctoral student during my first semester at Georgia Tech. Drs. Corbett and Beyah were pivotal in getting me through every moment of this program. Thank you both for the numerous "You can do it girl!" talks and many meals! I could not have prevailed without the "footsteps" from you both, and my heart is forever grateful.

I give my heartfelt appreciation and many thanks to Ashley Johnson and Calvin King, Jr. for helping me to study for our Ph.D. qualification exam. Furthermore, I could not have completed my research without the assistance and kindness of Sourabh Khire. I express my gratitude to Dr. Gary S. May, Dr. Bonnie Heck Ferri, Marilouise Mycko, Tasha Torrence, Jacqueline Trappier, Christopher Malbrue, LaJauna Ellis, and S. Gordon Moore, Jr. for their diligence and support throughout this process.

For over six years of professional experience and growth, I thank Ford Motor Company for the opportunity to flourish and to have an awesome career. Also, I thank

Michael Celentino for mentorship and allowing me to bring laughter into the office. I thank all of my former National Society of Black Engineers (NSBE) recruiting team members for countless memories.

Without question, I have been blessed with an abundance of friends that have been steadfast in my life. In completely random order, I would like to express my sincere gratitude to the following: Michael Coleman, Tamika Woodard, Christopher Patton, Vance Wilson, Aaron Davis, Masamba Moses, Creighton Fearrington, Adriane White Smith, Dr. Tyi-Sanna Jones, Tiffany Leflore, Tike Heshimu, William "T-S" Taylor, Walter Sutherlin, Jr., Tom Watson, Jason R. Smith, Tyrone Hamilton, Shewana Skinner, Angela Henderson, Shelby Stanley, Jaye Clarks, Kawana Melvin, Cheryl Barnett, Preston Harris, Jr., Melanie Womack, and Demeika Thompson.

I give immense thanks to Tina Clonts for always having an "open door" to me. I cannot find the words to convey my total appreciation for Tina's prayers, advice, listening ear, laughter, and encouragement throughout all of my experiences at Georgia Tech. Furthermore, I also extend my thanks to Dr. Donna C. Llewellyn, Dr. Marion Usselman., Dr. Jacqueline A. Fairley, Dr. A. Selcuk Uluagac, Dr. Aravind Kailas, Dr. Clyde A. Lettsome, Dr. Jeannie Lee, Dr. Ramanathan Palaniappan, the Black Graduate Student Association, Dr. Antoinette Thaxton-Brooks, Dr. Cyd G. Williams, and Elizabeth Baptist Church.

Without the unconditional love of my mother and biggest fan, Linda Harris, my academic pursuits and personal endeavors would have probably fallen much shorter. I thank my father, Clayton Mariner, for implanting a superior work ethic and sense of humor in me. To Aunt T, thank you for always having faith in me and for the many times

that we still cry laughing about grandma Ethel! I thank my younger brothers, Timothy Harris and T'Andre Harris, my godchildren, Tachelle McMillan and Lavon Hudginson, Jr. for always loving me just as I am. Know that *GOD*'s delay is not a denial…keep pressing!!!

Undoubtedly, I did not traverse the road to Ph.D. on my own. All of my achievements are due to *GOD*'s unmerited favor, and the support of many incredible people that were placed along my path. Even when I thought that this journey was complete, I was faced with a very unexpected and "beyond the scope" obstacle…but *GOD*! As I write my final words, I am overcome with so much joy. I am extremely proud to finally say, "I did it…now family and friends meet Dr. S dot Williams!!"

TABLE OF CONTENTS

LIST OF TABLES

LIST OF FIGURES

GLOSSARY

Anaplastic: refers to the lack of differentiation from normal cells and confirms tumor malignancy.

Anatomic Pathology (AP): the diagnosis of disease based upon the microscopic examination of organs, tissues, and whole bodies.

Antibody: a protein produced by the body's immune system in defense against a detected antigen.

Antigen: a foreign substance recognized by the body as potentially harmful including toxins, bacteria, viruses, or pollen.

Assay: a quantitative or qualitative test of a substance to check for the presence or concentration of infectious antibodies.

Atypia: the abnormality of a cell.

Clinical Pathology (CP): the diagnosis of disease based upon the laboratory analysis of bodily fluids.

Compression Ratio (CR): is defined by the ratio of the size of the original image to the size of the reconstructed image.

Diagnostic Losslessness (DL): a subjective and quantitative criterion that allows non-zero artifacts without compromising the image's diagnostic fidelity.

Hematoxylin and Eosin Stain (H&E stain): is a popular tissue-staining method used to determine the medical diagnosis.

Histology: the study of tissue or cellular samples using a light microscopic.

Histopathology: the microscopic examination of diseased tissue for the purpose of diagnosis.

Human Visual System (HVS): the biological part of the nervous system that processes visual detail.

Hyperchromasia: refers to an abundance of the deoxyribonucleic acid **(**DNA) that shows dark staining under examination.

Immunohistochemical (IHC): the process of detecting antigens in cells of a tissue section by exploiting the principle of antibodies.

Intraoperative: a process that is occurring, carried out, or encountered in the course of surgery.

Joint Photographic Experts Group (JPEG): established the image compression standard, which became the essential tool in the creation and manipulation of digital images.

Mathematical Losslessness (ML): an objective measure that results in a typical reduction in data on the order of 2:1.

Peak Signal to Noise Ratio (PSNR): an objective metric representing the ratio between the maximum possible power of an image and the power of corrupting noise due to image compression.

Microscopic Region of Interest (MROI): a partial section of a microscopic specimen that serves as the field of view of the microscope-imaging system.

Mitosis: the process of cell division including division of the nucleus and the fluid surrounding the nucleus.

Region of Interest (ROI): the pre-selection of identified boundaries of an object for a particular purpose.

Turnaround Time (TAT): time from which the pathologist receives the microscopic specimen to the time the diagnosis report is delivered.

Whole Slide Image (WSI): the digital representation of an entire microscopic-glass slide.

SUMMARY

When geographical distance poses as a barrier, *telepathology* is designed to offer pathologists the opportunity to replicate their normal activities by using an alternative means of practice. The rapid progression in technology has greatly influenced the appeal of *telepathology* and its use in multiple domains. To that point, *telepathology* systems help to afford teleconsultation services for remote locations, improve the workload distribution in clinical environments, measure quality assurance, and also enhance educational programs.

While *telepathology* is an attractive method to many potential users, the resource requirements for digitizing microscopic specimens have hindered widespread adoption. The use of image compression to address resource consumption is extremely critical to help advance the pervasiveness of digital images in pathology. For this research, we characterize two different methods that we use to assess compression of pathology images. First, our human-based method is characterized by the fact that image quality is human-based and completely subjective in terms of interpretation. Our second method involves image analysis, which is introduced by using machine-based interpretation to provide objective results. Additionally, the objective outcomes from the image analysis may also be used to help confirm tumor classification. With these two methods in mind, the purpose of this dissertation is to quantify the effects of image compression on data interpretation as seen by human experts and a computerized algorithm for use in *telepathology*.

CHAPTER I

INTRODUCTION

Technological advancements in telecommunications and the burgeoning need to convert medical information into a digital format have increased the number of applications within the field of telemedicine. Telemedicine involves the exchange of medical information from one location to another location by means of electronic communication to improve patients' health status [1]. For instance, a physician in a remote location who uses a “smart” phone to access a patient’s medical record is an example of telemedicine. The technological advancements in electronic communication offer services that include clinical treatment, consultation, digital-image transmission, remote-patient monitoring, and medical education. New developments in information technology have helped to bridge the physical gap between physicians and their distant patients. In practice, telemedicine is employed by the following two methods: store-and-forward and real time. The store-and-forward method involves the transmission of medical information (e.g., images) from one location to another. The primary benefit of the store-and-forward model is its asynchronicity because the receiving physician does not need to be readily available for transmission. On the contrary, the real-time model utilizes synchronous transmission and also helps to address mission-critical situations. While the significant advantage of using a real-time model over a store-and-forward model is obvious, the major tradeoff is the amount of resources that are required to conduct a session in real-time mode.

In technical terms, digitization enables an analog source to be converted into a digital format for viewing, storing, reproducing, and transmitting at a later time. The primary purpose for digitizing medical information is to aid the seamless transmission of patient-health data over varying distances using a telecommunications link. The initial design of a Picture Archiving and Communication System (PACS) was to help support a "filmless" environment in radiology. The PACS provides a network for reposition, viewing, and accessing multimodal images. Ultimately, the image-related information becomes accessible at any time from a remote location using telecommunication. In [2 - 3], authors noted that the quality of patient care would experience improvement through the provision of diagnostically-important images. Hence, telemedicine facilitated the branches of *teleradiology* and *telepathology* as a result of their inherent medical-imaging services.

Teleradiology, one of the most advanced disciplines within telemedicine, utilizes information technology to store and transmit digital-radiographical images. In 1993, the American College of Radiology and the National Electrical Manufacturers Association created the Digital Imaging and Communications in Medicine (DICOM) standard [4]. The DICOM standard ensures the interoperability of systems that are used for processing, sharing, and transmitting medical images. For example, a PACS is able to integrate and exchange information with other peripheral devices that are also DICOM compliant. Overall, the digital transformation has had a very positive impact on the workflow of radiology in the United States. James Thrall provided a comprehensive summary of *teleradiology* and its use in clinical practice [5 - 6]. In the United States, digitization in radiology has been a witness to pervasive use while the majority of radiology

departments have already converted themselves to a "filmless and fully digital" environment [7].

Similarly, several opportunities to exploit inefficiencies in the workflow of a pathology department also exist. With radiology serving as a paradigm, the use of digital images may become the routine for pathology diagnoses in the future [8]. In 1996, Weinberg defined *telepathology* as a subspecialty of telemedicine that involved the use of telecommunications technologies to transmit images to distant sites for the purpose of communicating diagnostic information or for teaching [9]. To address the need for standardization and interoperability in digital pathology, the DICOM Working Group 26 (WG-26) was established in 2005 and achieved a major milestone with the approval of Supplement 145 in 2010 [10].

Since 1986, *telepathology* has experienced growth in technological advancement and adoption despite the lack of an early digital-image standard. As a result of expanding healthcare networks and the opportunity to enhance the quality of service delivered to patients, the demand for utilizing information technology in the field of pathology has increased. The integration of such technology has encountered several challenges that include cost, image complexity, time consumption, and professional licensure. Today, *telepathology* manifests itself in several areas such as clinical diagnosis, consultation with subspecialists, quality assurance, and educational programs.

The remainder of Chapter 1 presents an overview and the basis for the research in this dissertation. Section 1.1 provides a succinct background of pathology and discusses the motivation to integrate digital imaging into the routine practice of pathology. Section 1.2 describes our models for both human-based and machine-based interpretation.

Section 1.3 of this chapter provides the statement of research. Section 1.4 concludes this chapter by outlining the contents of this dissertation.

1.1 PATHOLOGY HISTORY

Pathology is the study and diagnosis of disease through the examination of organs, tissues, bodily fluids, and whole bodies [11]. The practice of pathology is divided into the following two primary branches: Anatomic Pathology (AP) and Clinical Pathology (CP). CP is the diagnosis of disease based upon the laboratory analysis of bodily fluids. Examples of CP include hematology, microbiology, and cytogenetics. On the contrary, AP is the diagnosis of disease based upon the microscopic examination of organs, tissues, and whole bodies. Examples of AP include surgical pathology, cytological pathology, and forensic pathology. Histology is defined by the microscopic study of both tissue and cellular samples. In AP, histopathology is the examination of diseased tissue under a light microscope and foundation for determining the medical diagnosis.

The science of histochemistry involves the identification of chemical components in cells and tissues by way of a staining process. Thus, the application of staining provides illumination of tissue dissimilarities, as well as particular features of interest. The most popular microscopic-staining method used in histopathology is the hematoxylin and eosin (H&E) stain, which emphasizes the nuclear detail of a cell. Alternatively, immunostaining techniques that exploit the principle of antibodies have also been used to visualize specific antigens. Immunohistochemistry (IHC) refers to this process of detecting an antigen (e.g., bacteria) in tumor cells of a tissue section by using an antibody-based technique. In pathology, IHC is used to diagnosis specific types of

cancer and also requires a section of tissue. Tissue sections are removed from the human body in the following ways: biopsy and resection. Whereas a biopsy is the removal of a small section of tissue, a resection is the removal of an entire area of tissue (e.g., vasectomy).

With histopathological slides, fixation processes are done using the following methods: permanent section or frozen section. The permanent sections are formalin-fixed embedded tissue specimens that are mounted onto microscopic slides for staining. Moreover, a permanent section requires significant processing time of up to approximately 16 hours. Conversely, frozen sections are tissue specimens that are rapidly frozen during surgery, mounted, and stained with a processing time of approximately 10 minutes.

In 1997, Novis et al. determined that the intraoperative frozen-section technique had demonstrated its significant role in operative management [12]. To conduct an intraoperative consultation, a pathologist will examine a frozen section and render a subsequent diagnosis to the surgeon. Frozen-section examination affords several benefits such as determining the type of malignancy of tumor, assessing the surgical margins of the tumor, and identifying metastases to other tissues. In addition, the inherent nature of a frozen section frequently results in freezing artifacts that become noticeable on the processed slide. Such a conspicuous drawback is often tolerated by the surgical community in order to receive more expedited results at the time of surgery.

Undoubtedly, the frozen-section method is an invaluable tool and has a major impact on the care of a patient during surgery. Given the time constraints, the communication between the pathologist and surgeon must be cohesive to ensure a

reasonable turnaround time (TAT) for the intraoperative consultation. Using the aggregated data of the 700 institutions that participated in the Novis et al. study, the TAT to complete 90% of the frozen-section procedures was measured to be within 20 minutes [12]. The use of a light microscope is not always the most convenient or easily accessible means for examining a histopathological slide. Therefore, when computer technology became integrated with histopathological slides, digital pathology as a new means for pathology practice was born. In practice, a histopathological slide is converted into a digital image using a camera-mounted microscope or a slide-scanner system.

The use of digital images for diagnosis in pathology begets the question of how accurate is the interpretation compared to that achieved by using a traditional microscope. Conventional microscopy depends on visual inspection, which is intrinsically susceptible to both human errors and subjectivity. To facilitate more objective results, computer-aided tools that employ complex algorithms to automatically analyze the digital slides are used to augment the process for diagnosis. As the acquisition and digital quality of histopathological images continue to enhance the interpretation process, the use of digital images for clinical diagnosis stands to experience an increase in popularity.

1.2 PATHOLOGY IMAGE INTERPRETATION

For the purpose of this research, the word *interpretation* corresponds to the ability to evaluate morphological and molecular characteristics to help render the diagnosis of a histopathological slide in digital representation. Since an accurate *interpretation* far outweighs data compression, the employment of data compression must be balanced against the induced artifacts that could adversely affect the *interpretation* process. Moreover, the human-based *interpretation* of a histopathological slide can be subjective

and can also lead to inconsistent results in diagnosis. When viewing the same set of slides, the vast majority of diagnoses should be such that multiple pathologists would make the same diagnosis. When a tumor is unusual or has unusual features for which definitive criteria are partially lacking, then subjectivity in a diagnosis can become a factor. Furthermore, subjectivity has also been witnessed in tumor grading because of potential mitosis (i.e., division) or atypia (i.e., abnormality) of the nuclei. Often times, histopathological examination of slides can be a time-consuming task. Furthermore, the visual inspection of more complex pathology cases has the potential to require even more time for proper diagnosis.

As interobserver variability is already an existing concern within pathology practice, digital images may also afford another avenue for availing more quantitative analysis. Using machine-based tools to provide image analysis may also help to standardize *interpretation* processes in accordance with robust medical evidence. The provision of machine-based image analysis helps to extract morphological information, exploit image differentiations, and manage large databases.

The compression-related projects in this dissertation are separated into two models that assess the effects of image compression on *interpretation* of pathology images. For our first model, we carefully design an experiment that easily integrates within the pathologist's daily routine. The eight digital photomicrographs that establish our database for the human-based model are considered relatively easy-to-diagnose cases. Our human-based model assists the cultivation of a subjective metric to be used for the *interpretation* of compressed-histopathological images. For our second model, we assess the effects of compression on our machine-based algorithm used to extract glioma-image

analysis to potentially aid tumor classification. Our research goals aim to reduce the amount of human intervention, as well as the amount of image data in a diagnostically-acceptable fashion. Ultimately, we strive to enhance the transmission speed and decrease the memory footprint of the digital image without adversely impacting the final *interpretation* for diagnosis.

1.3 STATEMENT OF RESEARCH

The goal of this research is to develop quantitative criteria for image-compression techniques that result in high fidelity to afford confident interpretations of pathology information, and to aid the pervasive use of digital images in telepathology. The research in this work involves the conversion of microscopic slides to produce digital-microscopic images. Subsequently, we apply an image-compression technique to reduce the amount of data, and to allow more efficient allocation of required resources. The human-based study is conducted to collect subjective results from the pathology experts, and to establish a level of diagnostic losslessness (DL). Conversely, the machine-based study affords an objective perspective on data interpretation and produces the glioma-image analysis to potentially aid subsequent tumor classification. Moreover, the effects of compression on the glioma-image analyses are also studied to understand the potential impact on nuclear characteristics. Specifically, the research in this dissertation is captured in five remaining chapters, as summarized below.

- Telepathology: System Architecture and Applications
- Overview of Image-Coding and Visual Quality
- Human-based Study: Diagnostic Losslessness (DL)
- Machine-based Study: Nuclear Recognition and Morphometric Analysis

- Research Benefits and Future Recommendations

1.4 DISSERTATION OUTLINE

The remainder of this dissertation is outlined as follows: Chapter 2 comprehensively summarizes the progression of digital pathology and encompasses the details regarding the architecture and implementation of a telepathology system. Chapter 3 offers a fundamental understanding of image compression and illustrates how such a popular technique is employed in present practice. In addition, Chapter 3 also outlines the roles of color perception, cognition, and visual quality given the backdrop of digital-histopathological images. To understand the effects of image compression on data interpretation, Chapter 4 delineates our human-based study while our machine-based study is described in Chapter 5. In closing, Chapter 6 concludes this dissertation with recommendations for future research that involve image compression and image analysis for telepathology.

CHAPTER II

TELEPATHOLOGY: SYSTEM ARCHITECTURE AND APPLICATIONS

Chapter 2 encompasses the different architectures and implementations of a telepathology system. The growth of digital pathology is captured by summarizing numerous research efforts that are found in existing literature. In more recent years, the integration of technology has influenced the rapid evolution of digital pathology and telepathology.

The remainder of Chapter 2 is organized as follows: Section 2.1 discusses the primitive work and subsequent systems to illustrate the progression in telepathology. Section 2.1.1 and Section 2.1.2 describe the attributes of a Static-Telepathology System and a Dynamic-Telepathology System, respectively. Next, Section 2.1.3 presents an example of a Hybrid-Telepathology System. Then, Section 2.2 presents a brief discussion about the role of Virtual Microscopy. Finally, Section 2.3 concludes this chapter by discussing some of the challenges that exist for telepathology.

2.1 SYSTEM BACKGROUND

In 1968, the concept of using video microscopy to offer diagnostic pathology at a distance was first formally tested as part of the multiservice Massachusetts General Hospital-Logan Airport telemedicine project [13]. Over 20 years ago, the term "telepathology" was first described as the practice of pathology visualizing an indirect image on a television screen rather than viewing a specimen directly through a microscope [14]. Telepathology gained national awareness when a telepathology system

that was both dynamic robotic and real time was publicly tested. In 1986, a telepathology system incorporating color video and robotic microscopy was satellite-linked between Washington, D.C. and Fort Williams Beaumont Army Medical in El Paso, TX [15].

Additionally, telepathology also helps to establish a practical and faster communication link for remote locations that would otherwise experience a delay in receipt of information. For instance, such a link enables a rural hospital to take advantage of the expertise from outsourced subspecialty-pathology consultants. In the past, the primary application and most common use of telepathology was with the provision of intraoperative services [16]. In northern Norway, a unique hybrid dynamic-robotic/static-image telepathology system was created to offer frozen-section services to a remote hospital in 1991 [17]. The resident pathologist used a diagnostic workstation that was connected to the remote site by way of a telenetwork. Then, the images were transmitted as either live or still images over a 2 megabits/second link. The work done in northern Norway established the initial benchmark for using frozen sections in telepathology.

Digital pathology involves the creation and use of digital images to analyze and manage pathological information in an electronic environment. Telepathology equips a pathologist with the ability to view digital-histopathological images through a telecommunications medium from a remote location. Later in 2005, [18] presented a more simplified definition of telepathology that was expressed as “the processes of pathology using digital images.” More recently, however, other authors have defined telepathology from being a merely digital space by specifying that the digital-histopathological images are used to render a diagnosis [19 - 20].

Given the technological progression of digital cameras, several advantages of using digital photomicrography over conventional photomicrography have been achieved. The advent of digital photomicrography enabled editing, sharing, and viewing in a more efficient manner. In AP, microscopic specimens are prepared as either histological (e.g., tissue) or cytological (e.g., cellular) slides for further examination by a pathologist. Today, the creation of digital-microscopic images can be performed by using a camera-mounted microscope or an automated-slide scanner. A digital camera is only capable of capturing a limited area of the microscopic slide, and that particular limitation was resolved by the introduction of the automated scanner.

Alternatively, virtual slides are an attractive solution to allow the viewing of an entire microscopic specimen in a digital format. Dee et al. saw virtual slides as copies of microscopic slides in digital format that have been acquired at high-optical magnification [21]. With the technological advancements of automated scanners in recent years, a whole-slide image (WSI) is created to provide the digital representation of an entire microscopic slide. In the pathology community, virtual slide and WSI are synonymous with each other and have been used interchangeably in different literature [21 - 23]. Whole-slide scanners, which create WSIs, enable a substantial improvement in both image resolution and real-life simulation over camera-mounted microscopes.

The scanning resolution (i.e., microns/pixel) used to acquire a WSI correlates to the amount of information that will be visible in the digital image. When considering optical magnification and scanning resolution, as seen across various vendors of whole-slide scanners, a safe rule of thumb is that 20x = 0.46 to 0.50 μm/pixel and that 40x = 0.23 to 0.25 μm/pixel. Several advancements in technology have enabled the production

of image-capturing devices of much higher quality. To that end, a very comprehensive comparison of 31 commercially available systems that enable digital microscopy was published in 2006 [24].

Overall, telepathology affords the opportunity to improve the workload distribution in a clinical laboratory, conduct a teleconsultation between multiple sites, enhance processes for quality assurance, and augment educational programs. A telepathology system contains a microscope (e.g., conventional or robotic), an image-capturing device, a computer workstation at the host site, a computer workstation at the remote site, and a telecommunications link to connect the two sites. Moreover, a telepathology system can be utilized in the following three modalities: (1) Static or store-and-forward, (2) Dynamic, and (3) Hybrid.

2.1.1 Static-Telepathology System

Static or store-and-forward telepathology systems involve the capturing and transmission of still-image files. In simple terms, a digital photomicrograph is acquired at one site, and then sent to another site for further analysis. A static-telepathology system involves several still images selected by a pathologist and relies upon generic methods for transmission over the internet [25 - 26]. The most basic static system encompasses a light microscope that is mounted with a digital camera. A known benefit of this type of system is its simplicity and fairly low cost to implement. Inherent to static systems, the selected field or microscopic region of interest (MROI) for image capture depends on the referring pathologist.

Despite the benefit of simplicity, some issues of concern with a static system do exist. One significant problem area for static telepathology is the tissue sampling or field-

selection error [14, 16, 27 - 31]. For instance, the quality of an image is solely dependent on the experience of the person that captures the image. For the person performing the image capture, the mere inexperience with a digital camera may lead to several problems with the focus or color fidelity. In [17], Weinstein et al. suggested that the minimization of sampling errors may be achieved by assigning control of the microscope to the remote-telepathologist consultant. The confidence level of the consulting pathologist to render a diagnosis is affected by the quality of the digital slide. Furthermore, the limited amount of tissue-sampling area that is displayed in a MROI may also cause mistakes. As a result, several static images from a single case are usually required for examination.

As displayed in Figure 1, a whole-slide scanner may also be used to acquire a static WSI to be subsequently transmitted to another location [19]. A whole-slide scanner produces digital images of high quality while reducing the potential for field-selection error. Wilbur et al. discovered that using WSI technology helps to eliminate the selection bias of static images for teleconsultations [32]. Thus, a pathologist that is trained to examine the entire slide for diagnosis may find greater comfort in using a static system that supports WSIs.

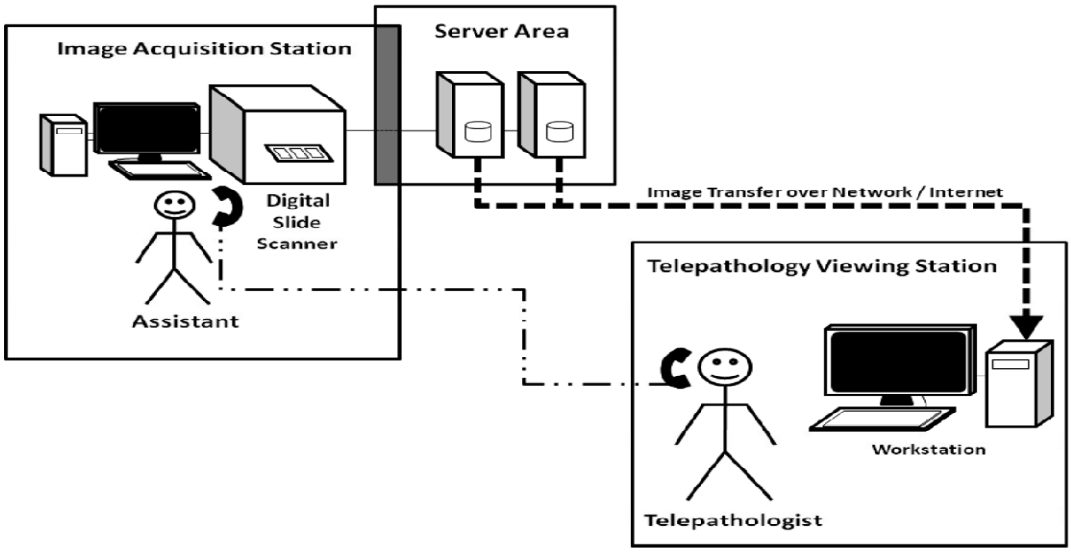

Figure 1. Static WSI is transmitted to a remote telepathologist.

2.1.2 Dynamic-Telepathology System

Dynamic telepathology enables real-time transmission of histopathological or cytological images. Using a dynamic system, digital images do not require the initial pre-capture for transmission at a later time, as with a static system. The dynamic mode affords video imagery in real time, and allows real-time interaction between the referring and remote pathologists. In practice, two types of dynamic-telepathology systems have been utilized over the years. In the simplest dynamic setup, the camera-mounted microscope is attached to a video network. As shown in Figure 2, the remote telepathologist is able to view the microscopic slide using a workstation and consultations can be facilitated in real time [19]. Over 10 years ago, Afework and his colleagues discussed their improvements to a digital-dynamic system that was used to simulate the behavior of a light microscope [33].

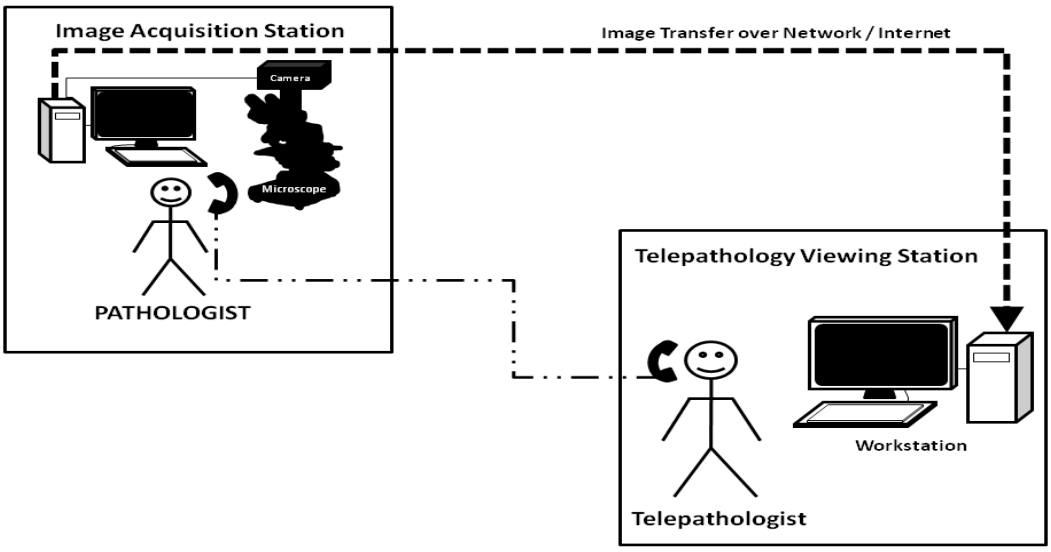

Figure 2. Dynamic mode allows real-time viewing and teleconferencing.

Beyond that, a more sophisticated dynamic system includes the remote control of the microscope through robotic means. In the telemedicine community, robotic telepathology marked the first use of a robotic interface [21]. The dynamic-robotic system has proven its enormous benefit by giving the remote pathologist real-time control over the robotic microscope. Thus, field selection, focus, slide manipulation, and other functions can be easily performed by the remote operator using the system's software interface. To facilitate real-time transmission, the image resolution in dynamic mode falls short in comparison to that in static mode. Several studies have reported that the employment of a robotic microscope helps to circumvent tissue-sampling errors, and also best emulates the traditional technique of using a conventional light microscope [29 - 30, 34]. While live mode is beneficial in numerous ways, such a system also requires a sizeable amount of bandwidth for transmission. As a result, the associated costs with implementing a dynamic system can be daunting and quite prohibitive depending on the application.

2.1.3 Hybrid-Telepathology System

A hybrid system is the simple combination of static and dynamic telepathology. In the mid 1990's, the United States Department of Veterans Affairs established a multi-hospital telepathology department to encourage the sharing of resources and pathology expertise [20]. The Veterans Integrated Service Network (VISN) is a network of medical centers and clinical facilities that has been grouped into 21 geographical regions within the United States. For example, the VISN-12 consists of eight medical centers and several community-based outpatient clinics located between the states of Michigan, Wisconsin, Illinois, and Indiana [35].

To provide routine surgical-pathology services to the Iron Mountain VAMC, a hybrid-dynamic/store-and-forward telepathology system was implemented [20, 36 - 37]. The Iron Mountain VAMC, which is located in the Upper Peninsula of Michigan, was the remote site that initiated the referral. The Milwaukee VAMC, which is located 220 miles away from the Iron Mountain VAMC, served as the host site that provided the laboratory services to the Iron Mountain VAMC. Therefore, the Milwaukee-Iron Mountain telepathology system consisted of bi-directional video conferencing to permit communication and diagnoses in real time. Additionally, the system also had the ability to operate in both high-resolution (i.e., static) and low-resolution (i.e., dynamic) modes. After reviewing a total of 2,200 cases over a 30-month time span, the two participating telepathologists helped to demonstrate that such a system had great value in providing routine diagnostic pathology services to a rural medical center [20, 36 - 37].

2.2 VIRTUAL MICROSCOPY

The separation between virtual microscopy and digital pathology involves the addition of tools to enable different views, annotation, and image analysis. While attempting to emulate a light microscope, virtual microscopy allows the operator to manage virtual slides (i.e., WSIs) by using a personal computer and appropriate software. Virtual microscopy far exceeds digital pathology by providing tools that enhance the pathologist's interface with virtual slides or WSIs. A virtual microscope performs many of the same functions as the light microscope including the selection of an objective lens magnification, and the ability to navigate across the tissue sample. Guzman and Judkins defined virtual microscopy as the ability to interactively examine a WSI with high resolution [38].

The use of a virtual slide or WSI has become quite prominent in both the education and proficiency testing arenas. Currently, a multitude of medical schools have already integrated the use of WSIs and virtual microscopy into their pathology courses. Weinstein et al. noted that the trend to become "fully digital" may produce a generation of pathologists who prefer the use of digital images over the traditional microscope [21]. In addition, virtual microscopy is also widely used for training and testing in the United States. For example, the American Board of Pathology has incorporated the technology of virtual slides into the process for certification [7]. The integration of virtual microscopy for obtaining licensure and certification forces pathologists to familiarize themselves with the technology. Furthermore, such a service has been mostly used by centers without an in-house histopathology laboratory.

The US LABS in Irvine, CA is an excellent example of a pathology laboratory that uses virtual microscopy and telepathology to redistribute pathology expertise [7]. The virtual slides are processed and stored on a server by US LABS. Subsequently, a hospital pathologist can then view the virtual slides remotely and analyze the results. Ferreira et al. implemented the "Virtual Microscope" that used a client-server architecture to surpass the functionality of a physical microscope [39]. Besides that, the "Virtual Microscope" also utilized pre-fetching and caching techniques to improve the efficiency of image retrieval.

2.3 CHALLENGES FOR TELEPATHOLOGY

Although telepathology offers a significant advantage in reducing the traditional transmission time for microscopic-glass slides from multiple days to minutes [22], several barriers have prevented the widespread implementation of telepathology. In 2002, Lee et al. mentioned that some of the critical constraints for telepathology were cost, resolution, time-consumption, and transmission of digital images [25]. The expenses that are associated with installing the components to enable digitization of microscopic slides are often hindrances to clinics or institutions with limited financial resources. In comparison to the traditional process, the scanning of microscopic slides also requires additional labor and processing time on the front end. The likelihood of an overly large file is a challenge that accompanies the idea of digital pathology. Undoubtedly, the transmission of multiple gigabytes of data is neither enticing nor practical in a clinical environment. As technology progresses, the marriage of size management and scanning speed will help to facilitate a more widespread embracement of digital images in pathology.

The subjective quality of a digital image is an important factor in relation to routine use in digital pathology and also remains susceptible to debate. For instance, the field selection, camera quality, microscopic settings, and observer's familiarity with viewing digital-pathology slides can be quite subjective and may affect the pathologist's ability to render a confident diagnosis. As another topic of discussion for telepathology, a practice that extends beyond the borders of a state is generating questions about professional liability and licensure [8].

CHAPTER III

OVERVIEW OF IMAGE-CODING AND VISUAL QUALITY

The goal of Chapter 3 is to provide a fundamental understanding of data compression and to illustrate a few techniques of data compression. Chapter 3 also discusses the role of color perception and provides a brief overview of visual quality in the context of digital-histopathological images. The goal for any compression technique is to minimize the data requirement without causing an unacceptable degree of error. In practice, an image-compression technique helps to decrease the quantity of information that is required to represent an image.

Chapter 3 is contained in eight remaining sections. Sections 3.1 and 3.1.1 represent background for the research focused in this dissertation. Specifically, Section 3.1 discusses the fundamental aspect of image sampling and quantization in digital representation of images while Section 3.1.1 describes sampling in relation to color images. Section 3.2 summarizes the roles of color perception, cognition, and visual quality in relation to image compression and pathology. Next, Section 3.3 offers a detailed overview of image compression. Section 3.3.1 summarizes Huffman coding, Lempel-Ziv-Welch (LZW), and run-length encoding (RLE) to delineate three examples of lossless-data compression. While Section 3.3.2 details the image-compression standard of the Joint Photographic Experts Group (JPEG), Section 3.3.3 describes the successive Joint Photographic Experts Group 2000 (JPEG 2000). Finally, Section 3.4 concludes this chapter by discussing the motivation for image compression, as it relates to telepathology.

3.1 IMAGE SAMPLING AND QUANTIZATION OVERVIEW

In signal processing, a "sample" refers to the observation of a signal at a particular point in time or space. Sampling is used to convert a continuous signal into a discrete signal by taking a series of samples, generally, at uniform intervals. The sampling frequency of a signal is defined by the number of samples per second, which is represented by the unit of hertz (Hz). Given an analog signal and its digital reconstruction, the well-known sampling theorem declares that the sampling rate must exceed twice the maximum frequency of the original signal. If a function is bandlimited, the theorem proves that a continuous signal can be reconstructed using a discrete sequence of samples to result in a framework that can still create an identical version of the original at the receiver.

In simple terms, an image is comprised of spatial coordinates (e.g., x and y) and the amplitude at the point of such coordinates. A digital image is defined by the use of discrete quantities to sample each of the (x,y) coordinate values and the amplitude. In image processing, as in digital pathology, discretization of the spatial coordinates is referred to as sampling while finite-bit digitization of the amplitude values is referred to as quantization. In practice, downsampling is done to decrease the spatial resolution of a digital image. Interpolation is the method by which the discrete inputs of neighboring pixels are used to estimate the output value of a particular pixel. In essence, interpolation allows the values at unknown locations to be estimated by using the data that is known. The problem of aliasing becomes a factor in the case of inadequate sampling and subsequent interpolation.

The digital illustration of an image attempts to reduce the total number of bits required to represent the source image without causing an unacceptable amount of noticeable error. This reduction in bits is accomplished in the following two ways: by minimizing the number of pixels in the image, and by decreasing the number of bits that are required to represent a pixel. In other words, a digital image is representation involves the processes of sampling and quantization (i.e., bits per pixel). Using sampling and quantization, the quality of a digital image is largely determined by the number of samples and discrete intensity levels. The sampling rate is automatically determined by the image-capturing device and is also used to calculate the bit rate by

$$BIT\ RATE = (\text{sampling rate}) \times (\text{bit depth}), \tag{3.1}$$

where the *sampling rate* is given in samples per second and the *bit depth* is given in bits per sample.

A digital image is represented in a binary format using eight bits for each pixel, where each pixel has $2^8 = 256$ possible values. The pixel resolution of an image is given in an M x N format, where "M" indicates the width dimension and "N" indicates the height dimension. For instance, an image that is 2048 pixels in width and 1080 pixels in height becomes $2048 \times 1080 = 2{,}211{,}840$ pixels or 2.2 megapixels. For the purpose of this research, we specifically focus on quantization because digital-microscopic images are typically pre-sampled at a specified and standard rate. Quantization helps to offer flexibility in the degree of compression for a given sampling rate. In fact, an important goal of this dissertation is to understand and propose favorable compression of digital-histopathological images.

3.1.1 Color Models and Color Sampling

Chrominance downsampling helps to optimize the bandwidth requirements by sampling the color information at a lower rate than that of the intensity information. With respect to the perceptual quality of an image, the human eye responds with greater sensitivity to luminance (i.e., brightness) in comparison to chrominance (i.e., color). The motivation for a color model is to facilitate the specification of a coordinate system and enable each color to be represented by a single point within that particular system. As one example, the RGB (e.g., red, green, and blue) color model consists of an intensity value for each of these three channels. The RGB model contains eight bits per channel, and often referred to as full color. An image with full color has a bit depth of 24 bits per pixel (bpp). For example, a full-color image with 1280 x 1024 pixels will produce a 31.46 megabits (Mb) file or a 3.93 megabyte (MB) file. While an intensity value of 0 for each channel results in the color of black (i.e., no light), full intensity for each channel results in the color of white (i.e., maximum light). Color models are often designed as hardware-oriented (e.g., liquid-crystal display (LCD) monitor) or application-oriented (e.g., Adobe Photoshop). The popular RGB model is commonly used with electronic devices that display images.

As a more advanced model, the YC_bC_r color space was created for digital imaging and video. More importantly, the YC_bC_r model allows an image-compression technique to take advantage of the luminance-chrominance characteristics of the HVS. The chrominance components are defined by the difference between a particular color and a "white" reference at the same luminance. The YC_bC_r model is separated into the following three components: Y denotes the luminance component, C_b denotes the

chrominance component for the blue difference (i.e., Blue – Y), and C_r denotes the chrominance component for the red difference (i.e., Red – Y). Consequently, the separation of the luminance from the chrominance is an important attribute of image compression that enables further reduction of the data.

Chrominance downsampling or subsampling is the process by which the color (e.g., C_b and C_r) information is encoded at a lower resolution than that of the luminance (e.g., Y) information. The various rates for chrominance downsampling are denoted by the following formats: 4:4:4 (e.g., 1x1 or no downsampling), 4:2:2 (e.g., 2x1 chrominance downsampling), 4:2:0 (e.g., 2x2 chrominance downsampling), and 4:1:1. In regard to the notation, the first number refers to the luminance channel while the second and third numbers refer to the chrominance channels. As shown by each format, the luminance channel remains unchanged during each downsampling level. Figures 3 - 6 are diagrams that illustrate the sampling rate for each chrominance-downsampling format. Most commonly, the Joint Photographic Experts Group (JPEG) employs the 4:2:0 chrominance-downsampling format, as described later in this chapter.

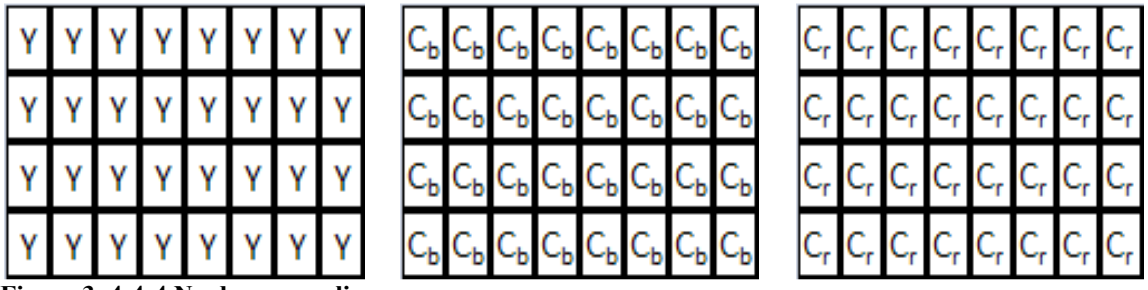

Figure 3. 4:4:4 No downsampling.

Figure 4. 4:2:2 Horizontal chrominance resolution is ½ sampling rate.

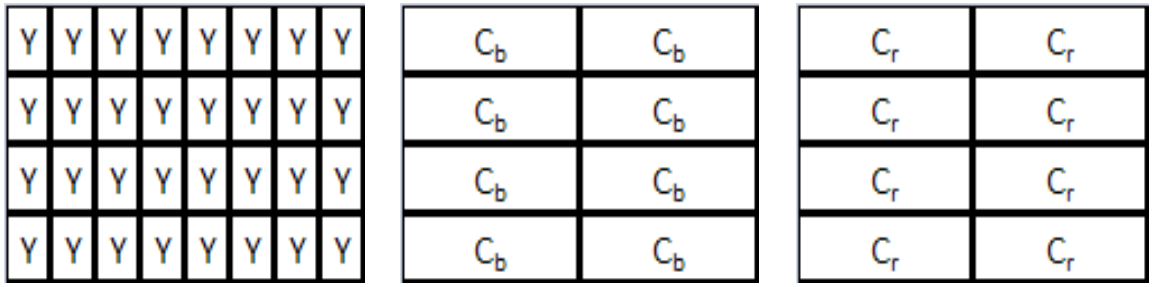

Figure 5. 4:1:1 Horizontal chrominance resolution is ¼ sampling rate.

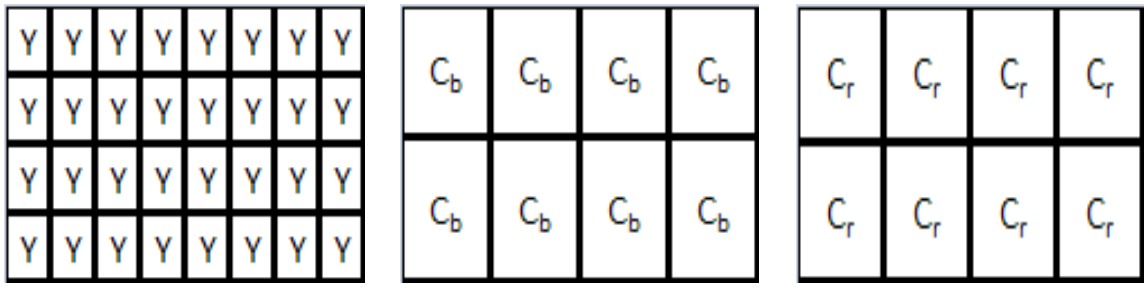

Figure 6. 4:2:0 Horizontal and vertical chrominance resolutions are ½ sampling rate.

In terms of compression, the conventional RGB color space does not offer the same benefit as with a luminance-chrominance model like the YC_bC_r color space. The difference is the fact that each of the channels in the RGB model carries some luminance information. Ultimately, chrominance downsampling helps to optimize the overall bit rate of a digital image by sampling the color information at a lower rate than that of the luminance information.

3.2 COLOR PERCEPTION, COGNITION, AND VISUAL QUALITY

We recognize that the human eye responds with greater sensitivity to luminance (i.e., brightness) in comparison to chrominance (i.e., color). Essentially, humans are most sensitive to changes in the visual information that is contained in the grayscale component or luminance. The human visual system (HVS) plays an important role in almost every aspect of our lives. With technological advancements and more ubiquitous applications, a significantly large amount of information can be represented in a digital format. While digital-image processing concentrates on the mathematical and probabilistic formulations, the complexity involved with visual perception has been studied to help develop techniques that are based upon the HVS. Thus, the visual mechanisms that are used in the perception of digital images are discussed in this section.

The human's ability to differentiate colors depends on the light-wavelength sensitivity of three types of cone cells with primary sensitivity of red, green, and blue light. In human vision, the eye responds to light wavelengths that fall within the spectrum of 400 nanometers to 700 nanometers. Specifically, the response of the eye is the greatest for the green wavelength followed by the red, and then the blue. The RGB color space is an additive model because the light from each color source is added together to produce the perceived color. The RGB representation consists of three primary phosphors (e.g., red, green, and blue) that are excited to stimulate the receptors (e.g., rods and cones) in the eye to generate the perceived color. Rods lack color-distinguishing ability and are responsible for night vision in humans. On the contrary, cones facilitate color perception and visual detection of finer details. To ensure adequate viewing under a microscope,

specimens are stained with certain colors to help reveal the cellular structures and components in histopathological sections.

Despite the fact that the RGB model is often used in image-display devices like computer monitors, the compression of color images is best performed using a luminance-chrominance model. To that end, the YC_bC_r model is well known for exploiting the fact that the HVS is more sensitive to variations in luminance than in chrominance. The YC_bC_r color model separates the luminance component, Y, from the chrominance components of C_b (i.e., blue-difference) and C_r (i.e., red-difference). Furthermore, the sensitivity to spatial variations in the two chrominance components is far more reduced in comparison to the sensitivity in the luminance component. Thus, the relationship between such color components and human vision is important for algorithms that employ data compression. The savings in valuable bandwidth is accomplished by reducing the sampling rate of the color components, which ultimately decreases the bit rate.

We recognize that psychovisual redundancy or irrelevance is addressed by exploiting the visual peculiarities of the HVS. The human eye does not perceive all of the visual information with equal sensitivity and regards some information as less important. Psychophysical experiments conclude that humans are more sensitive to high-spatial frequency components than to low-spatial frequency components. Visual acuity is defined by the acuteness of one's vision or ability to discern information. Furthermore, visual acuity measures the spatial resolution of the visual system.

With respect to compression, a compression technique accounts for the variations in visual acuity by separating the low-spatial frequency information from the high-spatial

frequency information of a digital image. While a test for deficits in visual acuity (e.g., color blindness) is not a requirement for a pathologist, the light microscope does contain ocular lenses to ensure that objects are examined in focus for accurate diagnosis. In theory, the HVS does not rely on the quantitative analysis of every pixel value in an image. The initial observation of an image produces a global impression to help form a cognitive representation of the image. Using that cognitive representation, the essential features are examined and extracted from the image.

The development of WSIs allows the pathologist to potentially "divorce" the microscope. As a result of such a "divorce", the physical distance between the pathologist and the microscope inspired a study regarding the cognitive skills and viewing process of a pathologist using virtual slides (e.g., WSIs). Krupinski et al. recorded the eye movements of nine observers with various levels of pathology expertise to trace the amount of visual "dwell" and "saccades" for each observer [40]. The study of eye movements helps to understand the cognitive processes between experts and novices in diagnostic pathology.

In terms of visual quality, the balance between compression-induced artifacts and visual quality of WSIs has not experienced rigorous investigation because of a few reasons. Johnson and fellow authors suggested that the large consumption of time and effort are both obstacles to such studies [41]. In addition, Johnson et al. evaluated a system to provide WSIs with diagnostic accuracy by employing compression schemes and display parameters that are based upon visual factors [41]. Additional research will help to understand the impact that compression schemes have on various types of WSIs to help improve the prediction of loss and provide more uniform visual quality.

Vision-oriented researchers realize the significant role of color perception, cognition, and visual acuity for both uncompressed and compressed images. Digital technology has taken some of this science into account by simply sampling the color information less frequently, as delineated in Section 3.1.1. The optimal method (i.e., future work) can take a more rigorous or unified approach. For pathology, the end-to-end use of a digital-histopathological image can be seen as a 3-step process that requires the following: 1) Preparation of the microscopic-glass slide by way of staining and fixation processes, 2) Production of the digital image by digitizing the microscopic-glass slide, and 3) Perception of the digital-microscopic image to facilitate confident interpretation and diagnosis. Ideally, all of the aspects that are related to visual perception of digital images deserve equal consideration with a unified perspective. The research in this dissertation, however, concentrates on the compression-specific effects in relation to the interpretation of digital-histopathological images. We utilize a well-recognized framework for compression of our digital-histopathological images in our experimental databases, and implement two different approaches to study the effects of image compression.

3.3 IMAGE COMPRESSION OVERVIEW

In theoretical literature, the process of using compression to reduce the amount of data is referred to as source coding. Such a reduction of data is classified as either reversible or irreversible. Image coding or compression is charged with removing the redundant or irrelevant data from an image. Image compression fulfills its mission to remove the nonessential information by using the following approaches: (1) Coding

redundancy (e.g., Huffman coding), (2) Interpixel redundancy (e.g., discrete cosine transform), and (3) Psychovisual redundancy (e.g., quantization).

The first approach, coding redundancy, is reversible and speaks to the fact that some pixel values or bit patterns are more probable than others. The second approach, interpixel redundancy, is also reversible and enables prediction of neighboring pixels given the frequent correlation between adjacent pixel values. The third approach, psychovisual redundancy is the concept used in quantization. Furthermore, quantization is irreversible and takes advantage of the human's sensitivity to different visual characteristics. Despite the loss of information due to quantization, a well-designed compression scheme possesses the ability to minimize the number of bits without introducing the image to significant distortion. This distortion can be measured mathematically, or ideally, by using psychovisual or subjective methods.

Additionally, an image-compression scheme is also beneficial because it helps to decrease the consumption of resources, such as the requirement for storage or transmission bandwidth. Image-compression algorithms are categorized as either *lossless* or *lossy*. For instance, *lossless* compression provides an identical reconstruction of the original image. An algorithm that employs *lossless* compression may be preferred for images that contain highly sensitive information, as with medical applications. In [42], Winokur et al. agreed to use the *lossless* method in their telepathology trial that included 64 uncompressed tissue slides, and a remote-microscopy system. On the contrary, *lossy* compression attempts to achieve the best quality for a given bit depth by producing an image that is as "close as possible" to the source image. The *lossy* method is tasked with determining which information is of lesser importance and discards that particular

information. The major downside to a *lossy* method is the potential for compression-induced artifacts, especially when applied at lower bit depths (i.e., <0.50 bpp). In essence, a compression artifact becomes visible because of the loss of information or quantity of bits.

The fidelity of an image can be assessed using the following two measures: objective measurement or subjective measurement. The signal-to-noise ratio (SNR), an objective measurement, is represented by the ratio between the original image and the corrupting noise caused by image compression. To that point, such noise will affect the image's fidelity and final representation. The peak signal-to-noise ratio (PSNR) value is used to evaluate the mathematical fidelity of the reconstructed image. Furthermore, the PSNR value is commonly used as a measurement for the quality of lossy-compressed images.

Specifically, the pixels of a reconstructed image are compared to the pixels of the corresponding source image in a pixel-by-pixel manner. For digital images, the error is the difference between the true (i.e., source) pixel value and the estimated (i.e., reconstructed) pixel value. The mean squared error (MSE) is the average of the difference in pixel error. PSNR is the ratio between the maximum possible power of a signal and the power of corrupting noise (e.g., MSE). In practice, a PSNR value of at least 30 decibels (dB) is typically indicative of good quality. The PSNR value for an image is computed by

$$MSE = \frac{\sum\left[I_{(i,j)} - C_{(i,j)}\right]^2}{M \times N}, \tag{3.2}$$

$$PSNR = 20 \log_{10}\left(\frac{MAX_I}{\sqrt{MSE}}\right), \tag{3.3}$$

where I denotes the source image that contains M x N pixel resolution, C denotes the reconstructed image, (i,j) represents the pixel location in each image, and MAX_I is the maximum possible pixel value of the source image.

Although the PSNR value has been a popular metric for image quality in the past, it has also suffered great criticism for not performing well as a predictor of image quality in the perceptual environment. The notion behind perceptual losslessness is that the distortion produced by image compression is invisible to the human eye [43]. A subjective measurement is obtained by using human observers to evaluate the perceptual quality of a digital image. Additionally, a subjective evaluation is considered very effective and reliable in assessing image quality, albeit often a time consuming and cumbersome task. A 5-point descriptive scale, known as the mean opinion score (MOS), is often used to subjectively measure image fidelity. In [44], an alternate method for subjective testing was introduced as a scale based upon perceptual impairment. In a perceptual model, the goal is often to achieve a level of just noticeable distortion (JND). JND is a subjective metric that attempts to utilize the lowest possible number of bits without sacrificing the amount of perceivable distortion. During our research, we implement subjective and objective measurements to compare how image compression affects the fidelity of our digital-histopathological images.

3.3.1 Huffman Coding, Run-Length Encoding, and Lemel-Ziv-Welch

Most lossless-compression programs generate a statistical model for the input data, and then use this model to map the input into bit sequences in such a way that more probable data will produce shorter output than the less probable data. As a result, the coding redundancy is reduced during the encoding process. In practice, the two types of statistical models are static and adaptive, with adaptive being the most popular. Lossless-data compression allows an exact reconstruction of the original data from the compressed data. This section presents three commonly used examples of lossless or reversible compression.

As a form of lossless or reversible compression, Huffman coding is used to address coding redundancy. Huffman codes contain the smallest number of possible code symbols, which are bits in the case of digital images. The reduction of the source occurs by ordering the symbols with their associated probabilities from top to bottom in terms of decreasing probability. To create the first source reduction, the lowest two probabilities are added to form a single symbol that equals the sum of those two symbols. Subsequently, the compounded symbol and its associated probability are also placed in the same manner to maintain the order of the most to the least probable. The process is repeated until the minimum number of symbols is reached and the final code is assigned.

Another commonly used lossless technique for data compression is the run-length encoding (RLE) method. In short, RLE seeks to reduce the physical size of a repeating string of characters. Such a string is referred to as a “run” and typically encoded into two bytes. The first byte represents the number of characters in the “run”. In practice, an encoded “run” may contain either 1 to 128 characters or 1 to 256 characters. Whereas, the

second byte is the actual value of the "run" and has a range of 0 to 255 in value. For example, "AAAAAABBBByyyCCC" can also be expressed as "6A4B3y3C". Following the RLE, the original 16-byte string would then be reduced to an 8-byte string of data to represent that exact same string. Thus, the RLE would yield a compression ratio of 2:1 in that case. The RLE technique is supported by bitmap file formats, such as Tagged Image File Format (TIFF), Bitmap Image File (BMP), and Personal Computer eXchange (PCX).

The Lempel-Ziv-Welch (LZW) algorithm is also a lossless technique for data compression, and a commonly used dictionary-based coder. A dictionary coder builds a table of strings, which are each assigned to a single code, to enable substitution of such strings with their corresponding codes. Using an uncompressed stream of characters, the LZW method creates a dictionary of character strings for subsequent reference. As the encoding process moves forward, the LZW algorithm identifies the repeated sequences in the data stream, and inserts them into the code table. When using 8-bit characters, the first $2^8 = 256$ codes only require a single byte and are assigned to the standard set of characters. To accommodate a total of $2^{12} = 4{,}096$ entries, the entire dictionary for the LZW-encoded data consists of 12-bit codes. After the first 256 entries in the dictionary, the remaining codes are assigned to "substrings", as the algorithm proceeds forward. Thus, the codes from 0 to 255 refer to individual bytes while codes from 256 to 4095 refer to substrings.

Initially, the LZW table contains codes for the first 256 entries, and the remainder of the table is empty. Subsequently, each new substring is added to the dictionary. If a substring has already been seen, then the LZW algorithm reads another character and concatenates that character with the current substring to create a new substring. Thus, the

next time that the LZW algorithm sees that particular substring again, the substring will then be encoded using a single number. With the LZW method, the longer the length and the greater the frequency of the sequence that is assigned to a single code, the higher the amount of yielded compression. The Graphical Interchange Format (GIF) is an image format that uses the LZW-compression technique.

3.3.2 Joint Photographic Experts Group (JPEG)

The Joint Photographic Experts Group (JPEG) created an image-compression standard that became the essential tool in the creation and manipulation of digital images. JPEG, a very popular standard, is a lossy technique used for image compression and ranks high for visual quality. To that point, JPEG is designed to be superior in recognizing the limitations of the HVS. The fact that the chrominance information is quantized more heavily than the luminance information allows JPEG to exploit the characteristics. Additionally, the option for a lossless mode in the JPEG standard does exist, but is not widely supported in existing products. The program that performs the encoding and decoding of a digital stream is known as a codec. Essentially, the JPEG standard defines the process by which a codec will achieve compression of a digital image. A diagram that highlights the key steps taken to obtain a JPEG-compressed image is shown in Figure 7.

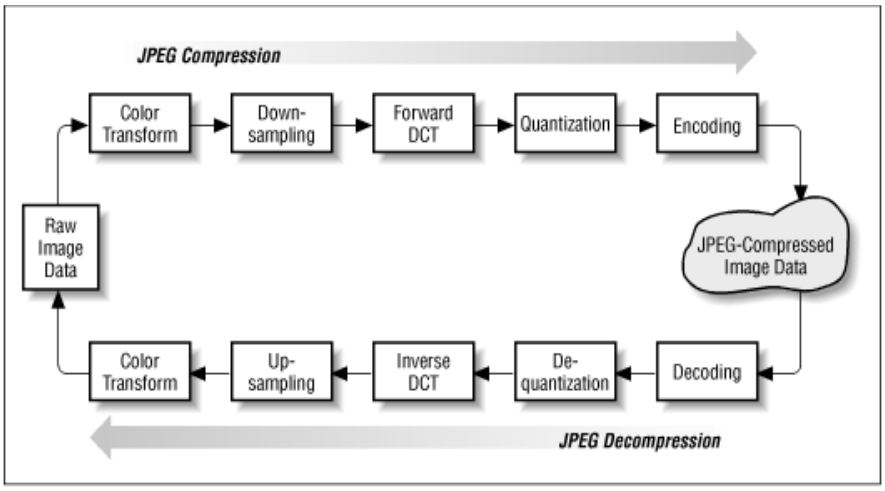

Figure 7. JPEG block diagram.

Initially, the first step in the JPEG diagram is to transform the RGB color space of the raw image. Subsequent to converting the RGB to the YC_bC_r color model, JPEG employs the 4:2:0 chrominance-downsampling format in the second step. The JPEG algorithm partitions the source image into matrix blocks of 8 x 8 pixels. The third step involves the discrete cosine transform (DCT) function to convert each of the 8 x 8 blocks into a frequency map. The DCT is a lossless or reversible method that addresses interpixel redundancy. Before the DCT conversion, the pixel values within each 8 x 8 block are shifted to be centered about zero. Using 8-bit pixel values, each pixel value is shifted by subtracting 128 from its original value. Thus, the original range of 0 to 255 for pixel values is then shifted to become a range of -128 to 127. With respect to the third step, Table 1 and Table 2 illustrate how each pixel value of the original 8 x 8 block matrix is shifted by a value of -128 just prior to the DCT stage.

Table 1. Original 8 x 8 matrix block of pixel values.

154	123	123	123	123	123	123	136
192	180	136	154	154	154	136	110
254	198	154	154	180	154	123	123
239	180	136	180	180	166	123	123
180	154	136	166	166	149	136	136
128	136	123	154	154	180	198	154
123	105	110	136	136	136	180	166
110	136	123	123	123	136	154	136

Table 2. Matrix block results after -128 shift of pixel values.

26	-5	-5	-5	-5	-5	-5	8
64	52	8	26	26	26	8	-18
126	70	26	26	52	26	-5	-5
111	52	8	52	52	38	-5	-5
52	26	8	38	38	21	8	8
0	8	-5	26	26	52	70	26
-5	-23	-18	8	8	8	52	38
-18	8	-5	-5	-5	8	26	8

After applying the DCT function, the 8 x 8 matrix block will then consist of 64 DCT coefficients. The top-left coefficient represents the lowest frequency in that particular 8 x 8 matrix block of the original image and is called the “DC” coefficient. On the contrary, the remaining 63 DCT coefficients represent the high-frequency information within that 8 x 8 matrix block of the original image and are called the “AC” coefficients. The DCT aggregates the low-frequency information into the top-left corner of the matrix,

which also addresses the fact that the human eye is most sensitive to low-frequency information and enables further encoding of the data.

While human vision is more perceptive of changes in luminance, the YC_bC_r color space offers the benefit of quantizing the luminance and chrominance channels separately. The fourth step in the JPEG diagram is to apply quantization, which is an irreversible or lossy method achieved by compressing a continuous set of values into a finite set of discrete values. Reducing the number of possible values of a quantity, thereby reduces the total number of bits that are required to represent such a quantity. For digital images, quantization is the process that determines which parts of an image can be discarded while minimizing the amount of actual perceived loss.

Psychovisual redundancy is manifested through the quantization stage. For JPEG compression, the user is required to utilize a quality factor (QF) using the numerical spectrum of 1 to 100. Furthermore, the QF has a direct correlation to which quantization matrix will be utilized for this process. Each of the 64-DCT coefficients is then divided by its corresponding coefficient in the quantization matrix and rounded to the nearest integer value. With respect to the fourth step, Table 3 is an example of the standard quantization matrix that is commonly used by JPEG. Furthermore, the degree of compression may be adjusted by multiplying the standard quantization matrix by the appropriate scaling factor prior to the division of each DCT coefficient.

Table 3. Standard quantization matrix for JPEG.

$$\begin{pmatrix} 26 & -5 & -5 & -5 & -5 & -5 & -5 & 8 \\ 64 & 52 & 8 & 26 & 26 & 26 & 8 & -18 \\ 126 & 70 & 26 & 26 & 52 & 26 & -5 & -5 \\ 111 & 52 & 8 & 52 & 52 & 38 & -5 & -5 \\ 52 & 26 & 8 & 38 & 38 & 21 & 8 & 8 \\ 0 & 8 & -5 & 26 & 26 & 52 & 70 & 26 \\ -5 & -23 & -18 & 8 & 8 & 8 & 52 & 38 \\ -18 & 8 & -5 & -5 & -5 & 8 & 26 & 8 \end{pmatrix}$$

The selected QF and corresponding compression rate are inversely related to each another. Thus, a QF of 1 produces the highest compression rate while a QF of 100 produces the lowest compression rate. The lower QFs generate larger coefficients in the quantization matrix and the converse is for the higher QFs. Subsequently, the coefficients are later used for division. A QF of 100 does not equate to exactly lossless compression, but does generate a reconstructed image that is excellent in approximating lossless. To that end, the user is able to adjust the amount of compression by simply controlling the QF for the image.

As a result of quantization, many of the high-frequency coefficients are typically rounded to zero while many of the remaining coefficients become small numbers that are either positive or negative. Given that the human eye is more critical to errors in low frequency, the reduction of information is done by discarding the high-frequency components. The quantization of a JPEG-compressed image lends itself to various types of distortion, which include the “ringing” and “blockiness” artifacts. After encoding each 8 x 8 block separately, the reconstructed image may experience discontinuities at the

boundaries of the blocks. Consequently, the "blockiness" artifact is a result of the quantization of such 8 x 8 blocks and becomes more visible at lower bit depths. The "ringing" effect is primarily because of the loss of high-frequency DCT coefficients. The generation of oscillations along the sharp edges in an image is a clear indication of the "ringing" artifact.

Typically, JPEG can achieve an image compression ratio (CR) of 10:1 to 20:1 without any visible degradation in the reconstructed image. Similarly, the CR of 10:1 to 20:1 can also be represented by 2.4 bpp to 1.2 bpp for full-color images. Figure 8 is an example of a raw (i.e., uncompressed) image compared to noticeable artifacts following the use of JPEG compression. In the second image, "ringing" is visible in several areas of the woman's hat and the edges of color contrast especially along the mirror. In the third image, the artifact known as "blockiness" is visible throughout the entire image.

Figure 8. Original image followed by visible ringing and blockiness, respectively.

Finally, the fifth step in the JPEG diagram is to use an entropy-encoding mechanism on the 8 x 8 matrix blocks, which now consist of DC and AC coefficients.

The remaining coefficients contain a large amount of redundant data, and entropy encoding will remove such redundancies in a lossless manner. The entropy-encoding algorithm creates a variable-length code table for encoding a source symbol using the estimated probability of occurrence for each possible value of the source symbol. Entropy encoding assigns codes to symbols, such that the symbols that occur most frequently will acquire the shortest codes. For JPEG, the frequently used entropy-encoding technique is Huffman coding.

3.3.3 Joint Photographic Experts Group (JPEG) 2000

An improved version of the JPEG standard was later introduced, known as JPEG 2000, which uses a discrete wavelet transform (DWT) coding standard. In contrast to the JPEG technique, the JPEG 2000 wavelet transform distinguishes the image as a wave, rather than small sets of discrete pixel values. Decomposition is performed by repeatedly taking the average between adjacent coefficients, which progressively produces a simplified version of the wave. The compression algorithm of JPEG 2000 uses the Embedded Block Coding with Optimized Truncation (EBCOT) scheme. EBCOT uses the wavelet transform to subdivide the original image into subbands. Furthermore, each subband is partitioned into smaller blocks known as code-blocks, which are coded independently.

The DWT also identifies significant and less significant variations within the image. In addition, JPEG 2000 is capable of operating at higher CRs (i.e., up to 300:1) without generating the common "blocky" and "ringing" defects of the original DCT-based JPEG standard. In comparison to traditional JPEG, the enhancement in compression afforded by JPEG 2000 also requires an increase in computational time.

JPEG 2000 has a rate-distortion advantage over its predecessor and also allows more sophisticated progressive downloads. The rate-distortion performance of JPEG 2000 is significantly better at lower bit rates, unlike traditional JPEG. Beyond that, another benefit is that users can also define a specific region of interest (ROI) within the image that can be randomly accessed for decompression with less distortion than other parts of the image. In recent studies, both JPEG and JPEG 2000 are used to analyze digital-histopathological images. Although we utilize the simpler algorithm of JPEG in our research because of its broad availability in software, our methodology of diagnostic-lossless compression will also extend to pathology systems that employ JPEG2000.

3.4 IMAGE COMPRESSION FOR TELEPATHOLOGY

The term "quality" can be quite relative to an individual's visual perception and remains susceptible to subjective analysis. More commonly than not, the threshold for acceptable quality of an image is dependent on the application. The utilization of an image is directly affected by the quality that is attributed to that particular image. Unfortunately, none of the existing measurements of image quality have been regarded as the single best approach across all applications. In the medical domain, the inherent loss of information that accompanies a lossy-compression technique does carry an enormous burden. The three general approaches that have been cited as measurements of image distortion in the medical arena are as follows: (1) SNR, as an objective measure of distortion, (2) Subjective rating, as a measure of image quality using psychophysical assessment, and (3) Diagnostic accuracy, as a perceptual measurement of distortion according to the image's use in clinical decision-making [45 - 46].

In the past, the majority of studies done on image quality were focused on intensity (i.e., grayscale) images. When compared to its predecessor, a chromatic (i.e., color) image is far more complex and requires much further computation than an intensity image. For instance, the tissue staining process, which uses color dyes and fluorescent agents, adds complexity to the image. Additionally, the file for a single digital-histopathological slide captured at high-power magnification (e.g., 40x) results in a massive amount of data. In 1997, Foran et al. noted that a digital-pathology image could easily contain 7 GB of data compared to only 25 MB needed to capture most relevant information for a radiology study [45].

In 2000, Marcelo et al. used 100 image samples that encompassed 10 different cases to study the use of JPEG compression in a static-telepathology trial [47]. However, Marcelo and co-authors used images with lower pixel resolution and did not include a quantitative analysis of quality-compression tradeoffs as described later in my research. Given the sensitivity of the color and molecular properties of histopathological images, an effective compression algorithm must ensure that the loss of data does not adversely affect the rendering of a diagnosis. To illustrate some of the degrading effects of compression on a digital-histopathological image, Figure 9 shows a comparison between a raw image and the reconstructed image after applying a CR of 74:1. As shown in the reconstructed histopathological image, the distortion caused by image compression can result in problems such as, severe discoloration, blockiness, and loss of nuclear detail.

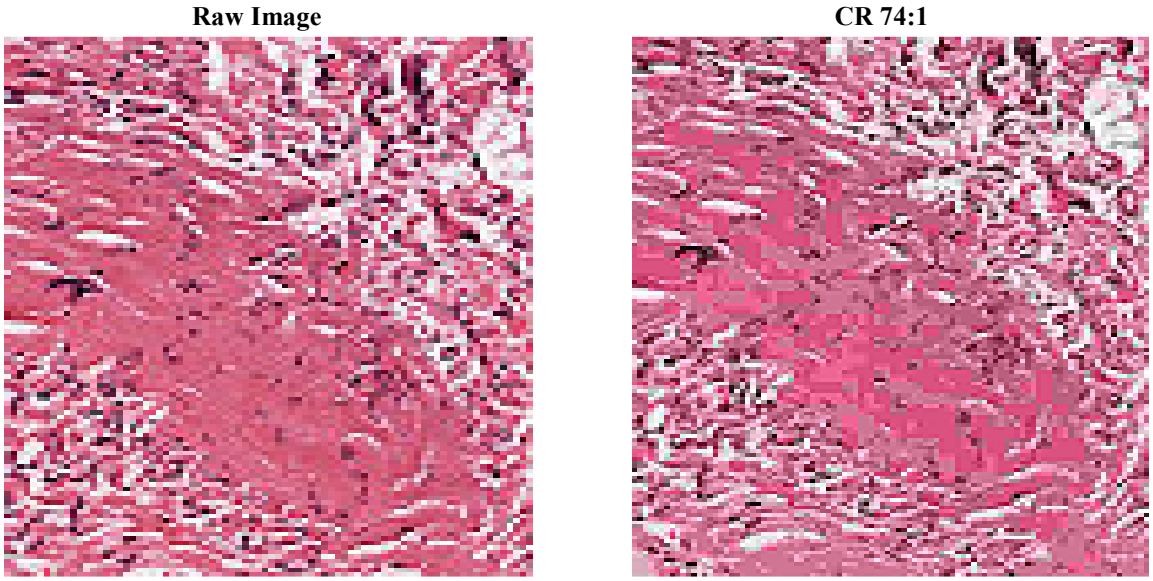

Figure 9. Raw image vs. reconstructed image at CR 74:1.

In 2010, Williams et al. applied image compression to digital-histopathological images to study the distribution of resources in an innately time-sensitive scheme such as pathology [48]. Furthermore, the digital-histopathological images were compressed using JPEG, as well as JPEG 2000 for analysis. Based on the 1-Stage and 2-Stage design in the study, each digital-histopathological image was annotated by a single pathologist to highlight the ROI that represented the essential information that was common to that specific diagnosis. While the 1-Stage Model only entails a single step, the 2-Stage Model is progressive and involves two steps to complete the process [49]. Khire reported that the 1-Stage Model offers a more competitive bit rate along with better workflow for pathology by not requiring human intervention to perform the initial ROI extraction [48 - 49].

Beyond the traditional 2-dimensional (2-D) image, the WSI offers better quality and is also expected to consume extremely large quantities of information. For example, a microscopic-glass slide of 20 mm x 15 mm in size may be scanned using a resolution of

0.25 μm/pixel, which is the target resolution for 40x optical magnification. The resulting WSI will contain a pixel resolution of 80,000 x 60,000 and equal almost 15 GB of data at 24 bpp. Although the standard for a digital image is 2-D, any type of digital-pathology image is considered 3-dimensional (3-D) with the presence of multiple focal planes. By convention, the optical axis is in the z-direction and focal planes are often referred to as "z-stacks" or "z-planes." Thus, a pathology image may consist of multiple "z-stacks" in order to represent a single sample of tissue. For instance, if the aforementioned WSI contained 25 focal planes, the file size would then increase from 15 GB to 375 GB.

The potential for exceptionally large data files is a concern for both 2-D and 3-D histopathological images, but our experiments concentrate on 2-D images. In this section, we presented a few examples to help describe the motivation for image compression of digital-histopathological images. In short, the sheer size of an image file is the key motivation to employ an image-compression technique, such as JPEG. The application of compression stands to improve the bit requirement and to facilitate more cost-effective management of digital images for telepathology. The research in this dissertation focuses on both the subjective and objective interpretations of JPEG-compressed images to enhance image analysis in pathology.

CHAPTER IV

HUMAN-BASED STUDY: DIAGNOSTIC LOSSLESSNESS (DL)

Chapter 4 provides the details about our human-based method to obtain quantitative and qualitative results from the participants in our experiment. Our initial experiment is the basis that we use to recommend our criterion that involves both image compression and our notion of diagnostic losslessness (DL). Chapter 4 is divided into three succeeding sections. Section 4.1 describes the experimental design and application of compression to achieve our diagnostic losslessness (DL) rate. While Section 4.2 discusses the constraints of our human-based evaluation, Section 4.3 closes this chapter with our conclusions of this study.

4.1 DIAGNOSTIC LOSSLESSNESS (DL) COMPRESSION

The first project that stems from the collaboration between Georgia Institute of Technology (Georgia Tech) and Emory University (Emory) is aimed at quantifying our criterion for data compression at a diagnostic losslessness (DL) rate. The DL criterion for image compression intends to offer a practical alternative to the more bit-demanding scenario of the mathematical losslessness (ML) rate of image compression. Typically, the CR associated with the ML rate is found to be on the order of 2:1 and preserves the data with very little to no perceptual degradation. Conversely, the higher teleconference-based CRs of 20:1 to 50:1 are considered too severe as a general rule for digital pathology. While ML provides a guarantee of excellent fidelity, histopathological images tend to necessitate a higher level of compression to become more practical for use in

telepathology. The desired level of image compression is that in which the artifacts, albeit non-zero, do not compromise the human-based interpretation of the image. To that end, a guiding criterion for compression at our DL rate is proposed using a human-based experiment with 2-D pathology images [50].

For our DL study, a SPOT Insight Digital Camera (Diagnostic Instruments, Inc.) is attached to a light microscope and used to acquire the digital photomicrographs of morphologically distinct lesions. Subsequently, our initial database consists of eight MROI images. The eight MROI images that we capture for our DL assessment are as follows: Anaplastic Thyroid Carcinoma, Brain Blastomycosis, Ovarian Yolk Sac Tumor, Paraganglioma, Pilar Cyst, Warthin's Tumor, Endometrial Cystic Atrophy, and Uterine Leiomyosarcoma. Figure 10 shows a snapshot of each MROI image that is contained in the database for our DL experiment. The MROI images are selected by a single pathologist from Emory and considered to have classical diagnostic features for the corresponding disease process. In addition, the MROI images range from 2x to 40x in optical magnification and consist of a 1600 x 1200 pixel resolution. Thus, the file size for each of the eight MROI images is 5.76 MB with 24 bpp.

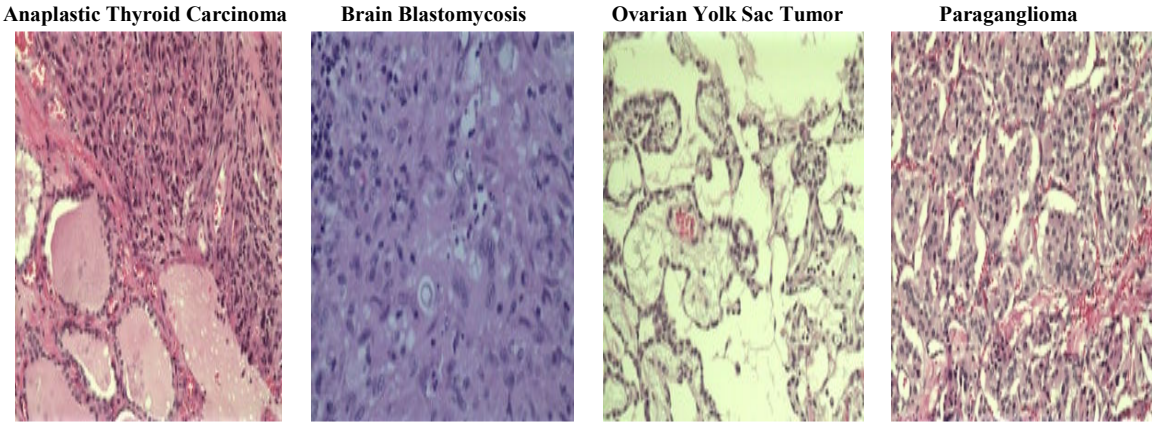

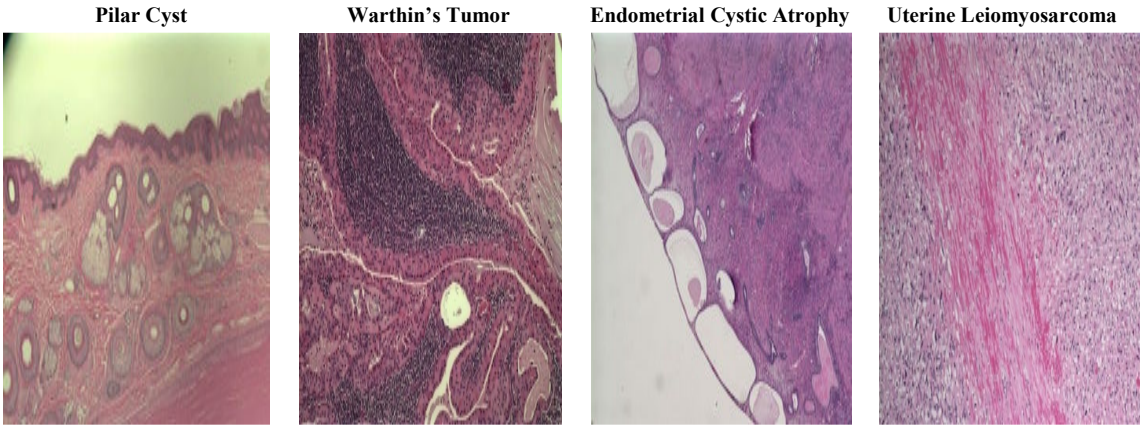

Figure 10. Uncompressed MROI images for the DL experiment.

JPEG compression is applied to each MROI image to achieve five different rates. Using MATLAB (The Mathworks, Inc.) to employ JPEG compression, each MROI image is compressed using the five following quality factors (QF): 75, 50, 35, 25, and 10. After using the QFs to employ multiple levels of JPEG compression, the CR ranges from 15:1 to 122:1. The "blind" test is administered using a no-reference image format because only the compressed images are being evaluated by each observer. A single session consists of the compressed images from only two of the MROI images. Furthermore, each compressed image is shown twice in random order to result in a total of 20 stimuli per session. To participate in the entire assessment and ensure that all 80 stimuli are evaluated, each pathology expert is asked to complete four sessions.

Our DL experiment consists of a total of 19 expert participants from Emory, which include 11 surgical pathologists and 8 pathology residents with at least 5 months of surgical-pathology training. The Blackboard Academic Suite (Blackboard, Inc.) software is used to create and remotely administer our DL test. With the Blackboard software, the participants from Emory can remotely access the "blind" test from any computer using a login and password [51]. The Blackboard design emulates the setting of a static-

telepathology system because the observers will view still images, as shown by the example in Figure 11. Upon completion of our DL assessment, a total of 80 stimuli will accompany subjective ratings by each expert participant. The participants are asked to rate each image based upon their ability to render the diagnosis of that image and to also provide qualitative comments. The assumption is that the MROI images contain minimal difficulty and are easy-to-diagnose cases. As a result, the actual diagnosis is not requested as a part of this test. During the test, images are rated using the following opinion scale: Acceptable (A), Somewhat Acceptable (S), or Unacceptable (U). Later, the opinion scale is used to calculate the Average Subjective Rating (ASR) using the numerical scale of 3.0, 2.0, or 1.0, respectively.

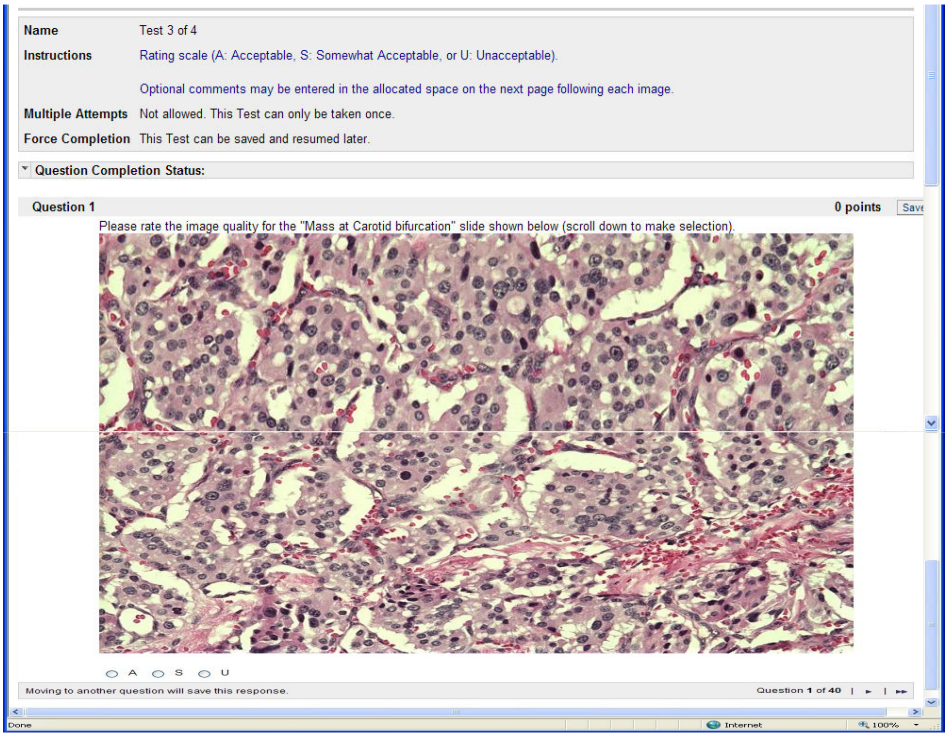

Figure 11. Example of DL test using Blackboard software.

Subsequent to JPEG compression, the CR range is from 15:1 to 43:1 across the entire set of 40 test images. The subjective scores for each of the 40 images are then used to assign a single ASR to each of the test images. For this experiment, an ASR of 2.5 or higher constitutes the achievement of DL for that particular image. The total of 40 test images are separated into two sets of 20 images referred to as Image Set 1 and Image Set 2, respectively. Table 4 and Table 5 display the results of the subjective evaluation and highlight the images that meet our DL criterion. The tables are populated with the values of ASR, DL, CR, and PSNR. Furthermore, the provision of such values will help us to evaluate the relationship between these measurements to determine if any inter-dependency exists.

Table 4. Image Set 1 results for the DL experiment.

Image Set 1	ASR	DL	CR	PSNR
Anap20x10	1.7		75	27.99
Anap20x25	2.6	√	43	31.68
Anap20x35	2.7	√	35	32.88
Anap20x50	2.6	√	28	34.04
Anap20x75	2.7	√	19	35.90
BrainBlast40x10	1.2		122	31.31
BrainBlast40x25	2.4		77	35.86
BrainBlast40x35	2.4		62	37.25
BrainBlast40x50	2.4		51	38.61
BrainBlast40x75	2.6	√	34	40.90
EndoCyst2x10	1.3		102	29.54
EndoCyst2x25	2.1		57	33.23
EndoCyst2x35	2.2		47	34.41
EndoCyst2x50	2.2		38	35.41
EndoCyst2x75	2.2		26	36.89
OvT10x10	1.5		64	27.05
OvT10x25	2.0		38	30.65
OvT10x35	2.0		31	31.86
OvT10x50	2.0		25	32.97
OvT10x75	2.1		18	34.69

Table 5. Image Set 2 results for the DL experiment.

Image Set 2	ASR	DL	CR	PSNR
Para20x10	1.9		59	26.67
Para20x25	2.7	√	34	30.18
Para20x35	2.7	√	28	31.31
Para20x50	2.7	√	23	32.38
Para20x75	2.7	√	16	34.01
Pilar2x10	1.1		97	28.32
Pilar2x25	1.9		54	31.60
Pilar2x35	1.9		43	32.56
Pilar2x50	2.1		35	33.40
Pilar2x75	2.1		23	34.79
UtLei4x10	1.1		58	26.01
UtLei4x25	2.2		32	28.91
UtLei4x35	2.2		26	29.77
UtLei4x50	2.1		21	30.52
UtLei4x75	2.1		15	31.73
Wart10x10	1.5		54	26.25
Wart10x25	2.4		31	29.34
Wart10x35	2.3		25	30.34
Wart10x50	2.6	√	21	31.28
Wart10x75	2.6	√	15	32.70

The results in Table 4 and Table 5 show that a definitive relationship between DL, CR, and PSNR cannot be established due to inconsistency in the performance of the MROI images. To that end, the results also confirm that the human-perceived quality of an image lacks a guarantee of correlation with the mathematically based PSNR value of the same image. Figure 12 and Figure 13 display the distribution of the ASR values for the test images in our DL experiment. As seen in these two scatter plots, the location of the cluster shows that the majority of test images only meet a threshold of "Somewhat Acceptable" or 2.0 for the ASR.

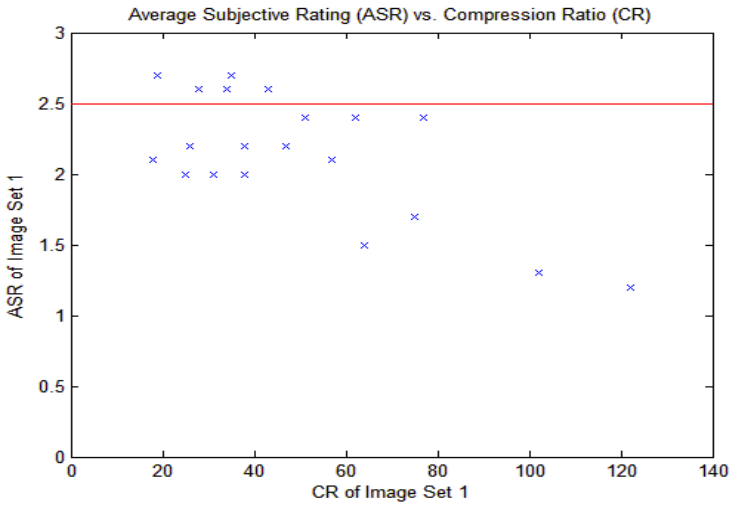

Figure 12. ASR vs. CR distribution for Image Set 1.

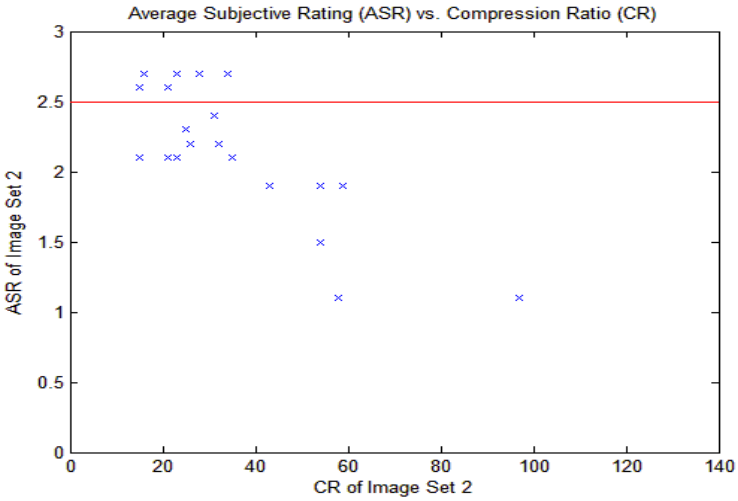

Figure 13. ASR vs. CR distribution for Image Set 2.

The interobserver variability considers the difference in subjective ratings across all 19 participants for each particular test image. For example, some observers may rate an image as acceptable for diagnosis while others may declare that same image as unacceptable. The participants are able to submit qualitative feedback along with their rating for each test image. As a result, the feedback that is most frequently reported for

poor ratings is as follows: lack of balance in color, insufficient nuclear detail, and too digitized or pixelated.

On the contrary, the intraobserver variability represents the total number of times that a single observer rates the same image differently within a single session. While a "mismatch" equates to a rating difference of one point, a "gross mismatch" equates to a rating difference of two points. To assess the intraobserver variability amongst the test images, the mismatches and gross mismatches are calculated for each observer, as shown in Figure 14. The results show that the observer with the highest variability for both types of mismatches (e.g., #4) is one of the surgical pathologists at Emory. Interestingly, the two observers with the lowest variability for both mismatches (e.g., #11 and #13) are pathology residents at Emory with three to four years of surgical-pathology training. We recognize that many factors contribute to the variability between all of our participants. Such factors include the participant's level of expectation regarding diagnostic detail, experience with using digital-histopathological images for diagnosis, variation in training, and interference due to environmental conditions while taking the test.

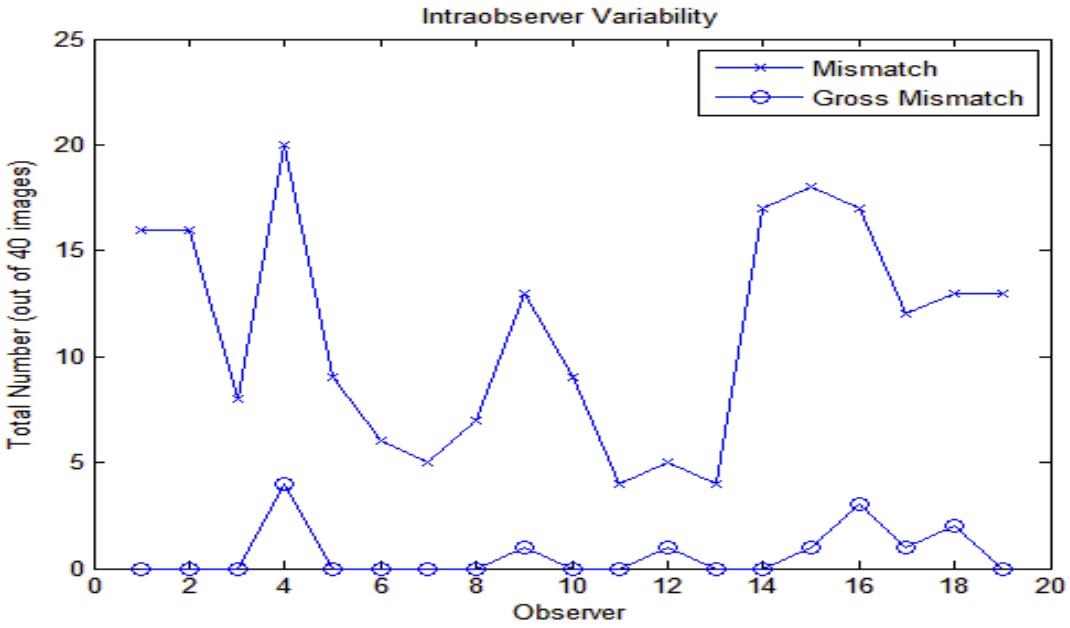

Figure 14. Intraobserver variability: Mismatch = 1 pt, Gross Mismatch = 2 pts.

4.2 QUALIFICATIONS

To minimize the amount of interruption in the varying schedules of our participants, we implement a web-based evaluation. This web-based design also allows us to share our evaluation with a much broader audience. While the Blackboard Academic Suite (Blackboard, Inc.) design is well executed and does enable remote access for our experts, our lack of control over the testing environment for each expert poses a few shortcomings. We recognize that the differences between the environments in which our "blind" tests are taken may affect the observer's rating of the MROI images. Such environmental drawbacks include the observer's physical location, external noise, room lighting, and resolution of the observer's monitor.

As with any static-telepathology system, the digital-microscopic image is prone to contain a dimension of variability. In practice, each MROI is captured by one pathologist and subsequently examined by another pathologist. The work flow and human factors to

consider include the following: (1) Preparation of the microscopic specimen from the cutting to the staining of tissue, (2) Use of the microscope to obtain optimal focus and contrast, and (3) Tissue sampling to select the region of tissue for image capture. Such considerations are also potential contributors to interobserver differences. For example, an image that is seen as inadequate by one pathologist may be seen as diagnostically acceptable by another pathologist. Nevertheless, given the practical importance of compression, the assessment of related effects on digital-microscopic images is valuable to the applications that use telepathology.

Initially, the results from this research provide us with important insight regarding the perceptual quality of compressed-histopathological images. We use the empirical data that we obtain from the participants as the groundwork for suggesting a level of compression that we coin as "diagnostic losslessness" or DL. As seen in Table 4 and Table 5, the test images that do meet our DL criterion have a CR that ranges from 15:1 to 43:1. We also notice that one of our test images does not meet our DL criterion at even the lowest CR. The variation in the subjective performances of our test images is related to errors that involve human factors. We suggest a CR of 10:1 for our DL criterion to include a margin of safety for error and variability. Furthermore, the 10:1 ratio supports a more conservative approach to image compression for the capture of digital-histopathological images.

4.3 EXPERIMENTAL CONCLUSIONS

To summarize our human-based study, our DL criterion of 10:1 compression is postulated as a viable tool for optimizing image compression of digital-histopathological slides [50]. In this study, the values of PSNR corroborate the common criticism that

PSNR alone is not a good predictor of perceived image quality. As seen in the previously shown Table 4 and Table 5, several of the images with high PSNR receive subjective ratings that are unfavorable and do not meet our DL requirement. In addition, this experiment also proves that the QF used to apply JPEG compression does not have a linear relationship with the corresponding CR that is consistent across multiple images. Using the same QF, one image may perform extremely well while another image may result in significant degradation. Following the complete evaluation, only four of the eight MROI images achieve our DL and are as follows: "Brain Blastomycosis" achieves our DL at a single compression rate, "Warthin's Tumor" achieves our DL at two compression rates, "Anaplastic Thyroid Carcinoma" achieves our DL at four compression rates, and "Paraganglioma" achieves our DL at four compression rates.

From Figure 14, the intraobserver variability is quite noticeable across all of the expert participants in this experiment. Furthermore, we suggest that the intraobserver variability is least dependent on the observer's level of pathology experience. For example, the participant's familiarity with viewing digital-pathology slides or the participant's testing environment may influence both interobserver and intraobserver variability. To address a few concerns, future improvements include the following initiatives: (1) The use of a camera with higher quality to capture images with more pixel resolution, (2) The extension of our MROI database by acquiring WSIs, and (3) The inclusion of histopathological samples that have an increased level of diagnostic difficulty. To preserve diagnostic quality, we recommend a more conservative and pragmatic CR of 10:1 as a favorable union between compression and interpretation of digital-histopathological images.

CHAPTER V

MACHINE-BASED STUDY: NUCLEAR RECOGNITION AND MORPHOMETRIC ANALYSIS

Chapter 5 discusses our machine-based study used to acquire glioma-image analysis with information on the morphological characteristics of nuclei and summarizes the results from our experiment. The remainder of Chapter 5 is organized in five remaining sections. Section 5.1 presents the motivation for image analysis. Section 5.2 covers the details regarding the specific characteristics and classification of diffuse gliomas. Section 5.3 discusses nuclear morphology and describes our methodology for automatically segmenting the nuclei for this study. Section 5.4 delineates the seven features of the morphometric group and provides a detailed review of their performance against image compression. Section 5.5 recaps our findings with regard to the effects of image compression on automated-nuclear analysis.

5.1 IMAGE ANALYSIS

In histopathological examinations, the detection of cellular activity is often performed manually, which is a labor-intensive task and suffers from subjectivity. The provision of objective information from computerized-image analysis will help to mitigate many problems associated with subjectivity in histopathological assessments. Furthermore, image analysis allows the acquisition of more complex and quantitative information about morphological features. Using computational methods for image analysis, the relationship between cellular behavior and experimental conditions can be assessed in large-scale images [52 - 53].

In 2009, Guzman and Judkins postulated that using a WSI encompasses the benefit of being able to perform complex image analysis as a supplement to everyday diagnosis [38]. As the use of digital images for primary diagnosis becomes more pervasive, the use of image-analysis tools will also earn more popularity. Such tools may potentially help to standardize many areas of cellular examination including the measurement of size, depth of invasion, percentage of certain cellular features, and mitotic counts of nuclei. In this study, our work involves evaluating the effects of image compression on machine-based analysis of WSIs. Our research goal aims to understand machine-based interpretation through the provision of nuclear-image analysis.

Moreover, we intend to examine the compression effects on the morphological characteristics of nuclei in diffuse gliomas. Specifically, a glioma is a type of tumor that originates in the brain. The term "diffuse" speaks to the fact that the tumor has the reputation of being extremely invasive. For the purpose of this research, we will utilize an image-analysis algorithm written in MATLAB (The Mathworks, Inc.) to automate the detection of nuclear boundaries and extraction of morphological features. With our machine-based experiment, the effects of image compression on nuclear detection, feature performance, and tumor classification will be assessed for diffuse gliomas.

5.2 GLIOMAS AND TUMOR CLASSIFICATION

Diffuse gliomas are the most devastating of brain tumors and well known for their infiltrative nature [54]. In practice, a pathologist will identify the characteristics of the tumor cells to determine the grade of the glioma. The tumor-grade system is used to classify cancerous cells in terms of their abnormality, as seen using a microscope. According to the World Health Organization (WHO), a grade I tumor is considered non-

malignant and categorized as well differentiated because the tumor cells resemble normal cells. A grade II tumor has moderate differentiation amongst tumor cells and can be malignant or non-malignant. A grade III is malignant with poor differentiation while a grade IV has very aggressive malignancy and is anaplastic (i.e., highly undifferentiated as compared to normal cells). For diffuse gliomas, only three WHO grades (e.g., II, III, and IV) are used to categorize the tumor from low grade to high grade. Given the abnormal growth of tumor cells in the central nervous system, a curative treatment for diffuse gliomas has yet to be discovered.

As the tumor grading of diffuse gliomas may experience inconsistency, the most difficult and significant problems regarding a histopathological diagnosis relate to the classification of the tumor [55]. The accuracy in classification and diagnosis are clearly fundamental to ensure proper management of patient care. To that point, diffuse gliomas often fall victim to misclassification because of the difficulty in distinguishing the tumor types. Infiltrative or diffuse gliomas are classified based upon their morphological criteria as oligodendroglioma, astrocytoma, or oligoastrocytoma (i.e., mixed). The glioblastoma multiforme (GBM), which holds a WHO grade IV classification, is the highest form of anaplastic astrocytomas. Figures 15 - 17 illustrate examples of each class of diffuse gliomas, respectively.

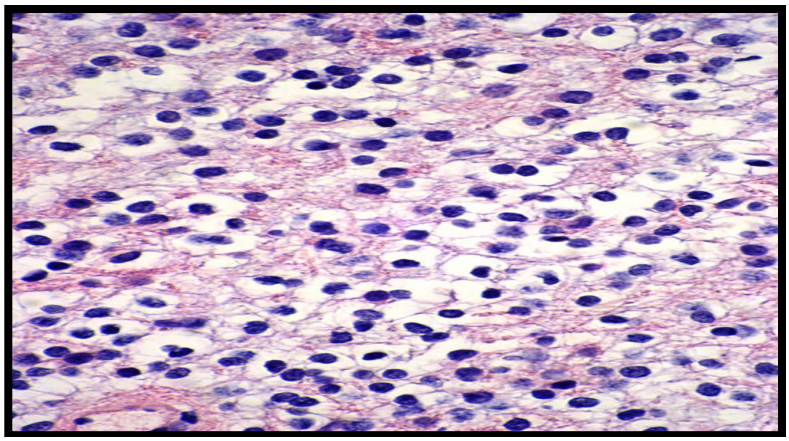

Figure 15. Oligodendroglioma tumor.

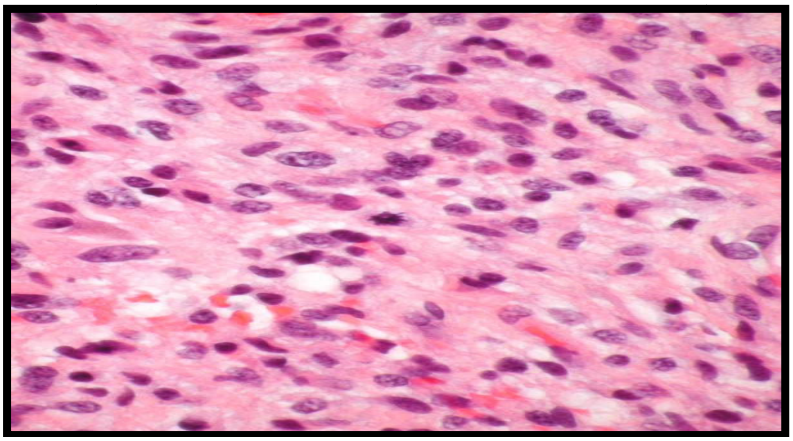

Figure 16. Astrocytoma tumor.

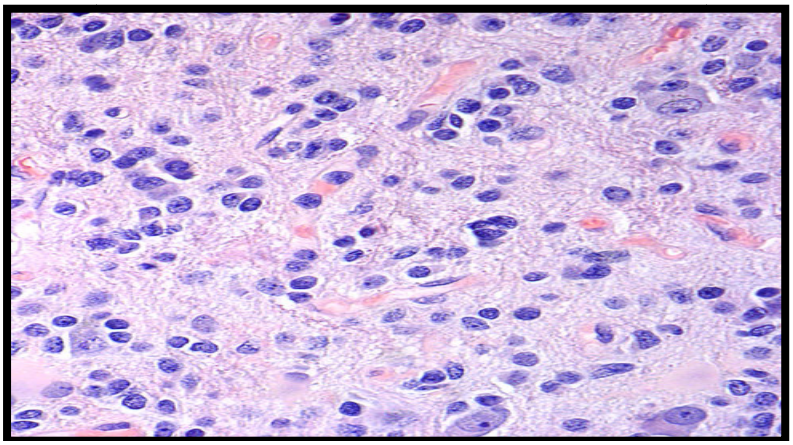

Figure 17. Oligoastrocytoma tumor.

5.3 NUCLEAR MORPHOLOGY

The shape, cytoplasm, and morphological characteristics of nuclei are used to differentiate cell types during a histopathological examination. With H&E staining, hematoxylin stains the nuclei blue while eosin stains the cytoplasm pink, as demonstrated by Figure 18. The cytoplasm, which is the fluid that fills the remainder of the cellular membrane outside of the nucleus, is not investigated for compression effects in this research.

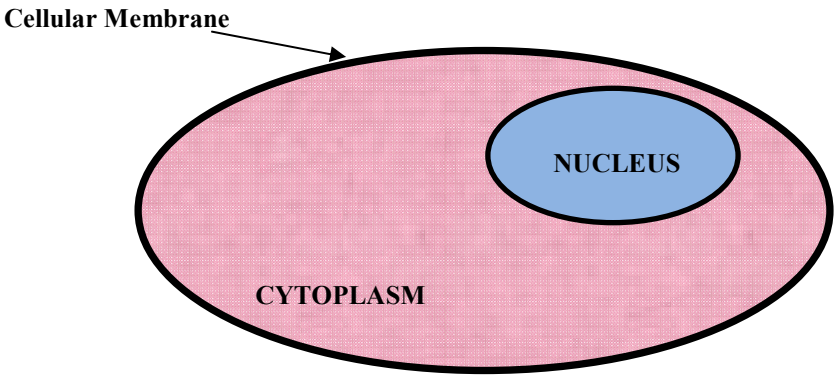

Figure 18. H&E stain illustrating colors for cellular components.

In practice, the diagnosis of diffuse gliomas primarily rests on the histopathological examination of H&E-stained slides [56 - 57]. The classification of diffuse gliomas is dependent on the shape and characteristics of the nuclei. Generally speaking, astrocyte cells are elongated, hyperchromatic (i.e., visibly dark-stained DNA), and irregularly shaped. On the contrary, oligodendrocyte cells are round in shape and more homogeneous. Using a tangible comparison, the nucleus (e.g., oligodendrocyte) of an oligodendroglioma resembles a "Florida orange", and the nucleus (e.g., astrocyte) of an astrocytoma resembles an "Idaho potato" [56].

Previously, several research studies have investigated the correlation between characterizing the nuclear features of importance with various cancer diagnoses [52, 58 - 62]. For our glioma-image experiment, we develop a multi-stage process to detect and segment the nuclei, collect the feature characteristics of nuclei, and assess the compression-induced effects on the nuclear analysis [63]. A Hamamatsu NanoZoomer 2.0 (Hamamatsu Photonics, K.K.) scanner is used to scan the microscopic slides, and to create 15 WSIs for our glioma database of 495 GB. Using the 3-tiered WHO grading system, the diffuse gliomas are selected to represent tumors from low to high grade. Our catalog of 15 glioma WSIs consists of the following:

- 2 - Astrocytoma (Grade II)
- 2 - Oligodendroglioma (Grade II)
- 2 - Oligodendroglioma (Grade III)
- 1 - Oligoastrocytoma (Grade II)
- 2 - Oligoastrocytoma (Grade III)
- 6 - Glioblastoma multiforme (Grade IV)

The original slides are scanned at 40x magnification, which is equal to a 0.23 μm/pixel scanning resolution of each glioma WSI. Subsequently, each glioma WSI is also divided into image tiles to enable more efficient processing by using smaller images. The image tiles are scanned at 20x magnification, which is equal to a 0.46 μm/pixel scanning resolution. The image tiles contain a pixel resolution of 4096 x 4096. For convenient use across multiple applications, the image tiles are stored in TIFF format without any compression.

The number of tile images per glioma WSI is dependent on the size of the tissue specimen in the glioma WSI. In other words, more tile images are required to represent a larger specimen that is present in the glioma WSI. To ensure a majority amount of tissue presence, each image tile is measured against a tissue threshold of 80% prior to any further analysis. Once the raw-image tiles are selected based upon their proportion of tissue, the image tiles are processed to identify the nuclei. Table 6 shows the total number of image tiles for each glioma WSI, the percentage of raw-image tiles that meet the tissue threshold, and the total number of nuclei that are identified as the raw count. Using the first image as an example, only 14% of the raw-image tiles are processed and represent a total count of 26,592 nuclei. With respect to the image tiles from our glioma WSIs, we process 47% of all image tiles or 2,664 image tiles, and segment over 7.3 million nuclei.

Table 6. Total number of tiles processed for nuclear analysis.

WSI	# Tiles	Processed	# Nuclei
astroII.1	56	14%	26,592
astroII.2	72	39%	62,112
oligoII.1	240	48%	696,254
oligoII.2	162	31%	320,840
oligoIII.1	288	52%	718,201
oilgoIII.2	324	66%	1,996,715
oligoastroII.2	204	55%	802,573
oligoastroIII.1	162	28%	438,163
oligoastroIII.2	180	54%	470,014
gbm0.1	81	63%	376,946
gbm0.2	144	35%	408,515
gbm1.1	351	55%	504,754
gbm1.2	120	51%	172,936
gbm2.1	144	20%	257,226
gbm2.2	136	27%	101,132
	TOTALS		
	2,664	47%	7,352,973

5.3.1 Nuclear Segmentation

Following the acquisition of the reduced set of raw-image tiles, the nuclei are segmented using the approaches of edge detection and watershed transform. In digital images, segmentation is often achieved based upon discontinuities in intensity values. The discontinuities in intensity can be witnessed through points, lines, and edges [64]. The combination of edge detection and thresholding result in a binary image that shows a distinct separation between the foreground pixels and the background pixels. After generating a binary mask for each image tile, we apply global thresholding by the definition

$$I(x,y) = \begin{cases} 0\ (black), & if\ f(x,y) < T_I \\ 1\ (white), & if\ f(x,y) \geq T_I \end{cases}, \tag{5.1}$$

where $I(x,y)$ represents the thresholded image, $f(x,y)$ is the binary mask of the source image, and T_I is a constant value determining the global threshold. The pixel values of the foreground are set to equal 1 and the pixel values of the background (i.e., everything else) are set to equal 0. Figure 19 depicts an image tile that has undergone nuclear segmentation to highlight the nuclei that were captured during the process.

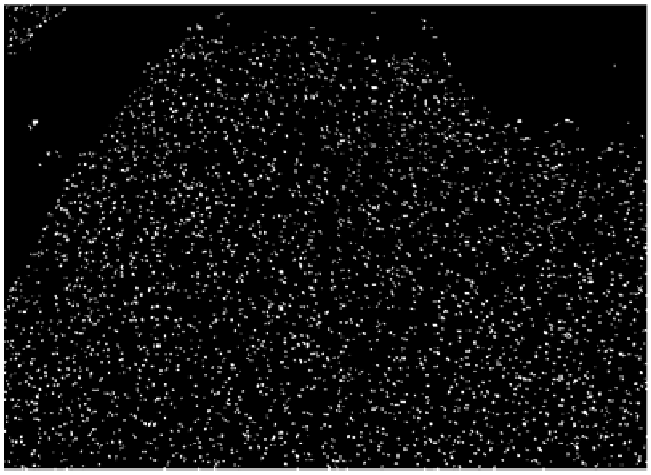

Figure 19. Binary image showing segmentation of nuclei.

The segmentation process is prone to errors such as over segmentation and under segmentation. The watershed transform is employed as a means to address such inherent problems. Using the binary mask, the goal is to combine the over-segmented nuclei and to capture the under-segmented nuclei. A watershed is the divide or ridge that separates two areas of land that are drained by different river systems. A catchment basin is represented by the geographical area that is draining into a river system. Essentially, the watershed transform determines the ridge and catchment basin of the binary image. As a result, the original image is then re-segmented with new nuclei being identified in the catchment basin. Furthermore, the watershed transform also helps to resolve the issue with overlap in morphological features of nuclei, which is quite common for diffuse gliomas.

5.4 COMPRESSION AND MORPHOMETRIC ANALYSIS

Morphometric analysis is another manifestation of an objective technique that can be used independently of human evaluation to examine a cellular assay. Moreover, morphometric analysis enables one to describe complex shapes in a rigorous fashion, and

permits numerical comparison between different morphological features. Machine-based analysis has aided the classification of nuclei through assessment of various features such as area, elongation, eccentricity, sphericity, intensity, texture, and contour [58 - 60]. The parameters associated with an ellipse are often used to model nuclear features for quantitative analysis. For our research, the morphometric group consists of the following seven features: area, perimeter, eccentricity, circularity, major axis length, minor axis length, and extent.

- Area – total number of pixels that belong to a nucleus.
- Perimeter – total number of pixels that lie along the boundary of a nucleus.
- Eccentricity – ratio of the major axis length to the minor axis length of a nucleus, where 1 is a maximum ellipse.
- Circularity – a function of the area and perimeter of nucleus.
- Major Axis Length – pixel length of the longest diameter of the nucleus.
- Minor Axis Length – pixel length of the shortest diameter of the nucleus.
- Extent – ratio of the pixels in the nucleus to the pixels of the smallest rectangle that contains the nucleus, as function of area.

For our compression analysis, we analyzed the effects of eight different CRs by using the following QF values: QF = 100, 94, 70, 50, 30, 20, 10, and 5. The nuclear correspondence between the raw and compressed images must be established prior to comparing the morphometric analyses. To determine if a nucleus that is detected in the raw image corresponds to a nucleus that is detected in the compressed image, the ratio between the two nuclei is written as

$$\frac{intersection\ (N_1,\ N_2)}{min(Area_1,\ Area_2)} \geq BT \tag{5.2}$$

where N_1 and N_2 denote the individual nuclei that have been detected in the raw and compressed images, respectively, $Area_1$ and $Area_2$ are the calculated areas for each nucleus that has been detected in the raw and compressed images, respectively, and BT represents the boundary threshold that must be met to achieve nuclear correspondence the raw and compressed images. After the nuclear detection and correspondence matrix are both complete, the nuclear analysis is employed to form the feature vector for the morphometric group.

Given that the morphometric features of nuclei pose as good descriptors of nuclear morphology, the process of nuclear detection within our algorithm must afford accurate recognition of the nuclear boundaries. Thus, the accuracy in nuclear detection is also measured against nuclear distortion subsequent to applying image compression. The compression-induced effects have a direct impact on the construction of the nuclear boundaries. Nevertheless, segmentation is performed on the compressed images despite the potential for compounding the amount of distortion. Table 7 summarizes the four types of nuclear distortion that are attributed to image compression in this study.

Table 7: Types of nuclear distortion.

Distortion Type	Details
False Positive (FP)	Nucleus in compressed image does not correspond to nucleus in raw image
False Negative (FN)	Nucleus in raw image does not correspond to nucleus in compressed image
Merged	Multiple nuclei in raw image correspond to single nucleus in compressed image
Split	Single nucleus in raw image corresponds to multiple nuclei in compressed image

The four types of distortion that are presented in Table 7 are specific to boundary detection. In other words, only the edges of nuclei are important in the cases of "FP", "FN", "Merged", and "Split". Conversely, all of the features within the morphometric group consider some of the internal properties of the nuclei with "Perimeter" as the exception. While all of the distortion types and morphometric features are vital to our glioma-image analysis, we will also gather information about the robustness of our algorithm. Our algorithm is designed to provide faster, objective, and reproducible analysis subsequent to machine-based interpretation of the nuclear features. With the increasing demand to employ an image-compression technique, a comprehensive understanding of compression effects will allow us to ensure that the integrity of our analysis is not compromised.

5.5 EXPERIMENTAL CONCLUSIONS

To encompass the 3-tiered WHO grading system, we select three of the glioma WSIs to discuss in this section. The three glioma WSIs are as follows: astroII.2, oligoIII.2, and gbm0.2. For the experimental conclusions, all of the percentage values are

rounded to the nearest tenth. The graphical results and subsequent conclusions for these glioma WSIs are elucidated in three subsections titled by the name of each glioma WSI.

The graphs for nuclear detection, distortion, and morphometric error are only presented once in this section. We use "astroII.2", the first of the three glioma WSIs, to illustrate how the nuclei respond to the eight different levels of compression. We are able to assess the initial effects of compression on the nuclear shapes by simply considering each distortion type. Subsequently, we focus on the features of "Eccentricity" and "Circularity" to help confirm whether the nuclear classification is astrocyte or oligodendrocyte. We use scatter plots to help express the correlation between "Eccentricity" and "Circularity" for each of the three glioma WSIs.

To visualize how our algorithm identifies and segments the nuclei in different types of glioma WSIs, we tabulate the three examples from this section. Table 8 details the nuclear count along with the four types of nuclear distortion for both low and high compression. In Table 8, "Low ACR" is used to assess nuclear performance at a level that is equivalent or closely equal to the DL rate and ranges from 8:1 to 11:1. Conversely, "High ACR" represents the maximum level of compression and ranges from 57:1 to 67:1. To that end, Table 8 delineates these two extreme measures to illustrate how compression influences the accuracy of our algorithm in terms of nuclear-boundary detection.

Table 8. Nuclear count and distortion types for low and high compression. (Percentages are rounded to the nearest tenth.)

Astrocytoma (Grade II): astroII.2			
	Raw (ACR 1:1)	**Low (ACR 11:1)**	**High (ACR 67:1)**
	62,112	58,203	54,398
Loss	0.0%	6.3%	12.4%
FN	0.0%	6.0%	12.2%
FP	0.0%	1.5%	50.1%
Merged	0.0%	0.5%	1.3%
Split	0.0%	0.4%	1.8%
Oligodendroglioma (Grade III): oligoIII.2			
	Raw (ACR 1:1)	**Low (ACR 10:1)**	**High (ACR 66:1)**
	1,996,715	1,879,961	1,566,092
Loss	0.0%	5.8%	21.6%
FN	0.0%	5.3%	21.0%
FP	0.0%	0.9%	9.7%
Merged	0.0%	1.6%	3.2%
Split	0.0%	1.3%	3.7%
Glioblastoma multiforme (Grade IV): gbm0.2			
	Raw (ACR 1:1)	**Low (ACR 8:1)**	**High (ACR 57:1)**
	408,515	387,351	333,693
Loss	0.0%	5.2%	18.3%
FN	0.0%	4.9%	18.0%
FP	0.0%	0.9%	8.2%
Merged	0.0%	2.0%	4.1%
Split	0.0%	1.8%	4.3%

Astrocytoma (Grade II): astroII.2

The first effect of image compression that is observed is with the identification and segmentation of nuclei, which enumerates the total count of nuclei. Due to the potentially vast amount of image tiles, the average compression ratio (ACR) for the corresponding set of image tiles is used as the standard for each glioma WSI. Image compression is applied at eight different rates and the ACR ranges from 4:1 to 67:1 for the "astroII.2" example. In our attempt to achieve 10:1 compression, we apply a QF = 94 to each glioma WSI. For "astroII.2", we obtain an ACR value of 11:1 instead of 10:1. Figure 20 shows the loss of nuclei as a direct result of each ACR. The raw count for the

nuclei is 62,112 and the loss of nuclei ranges from 6.3% to 12.4%. In theory, the expectation is that an increased degree of compression would also increase the percentage of nuclear loss. For the ratios between 34:1 and 40:1**,** the relationship between compression and nuclear detection is reporting behavior that is opposite of what we expect for the relationship between these two characteristics. To that extent, the line in Figure 20 should display a continuous increase in slope. We do not fully understand the cause for the abrupt decrease in the slope. Later in this chapter, we discuss the potential sources that may contribute to the unexpected behavior that is shown in Figure 20.

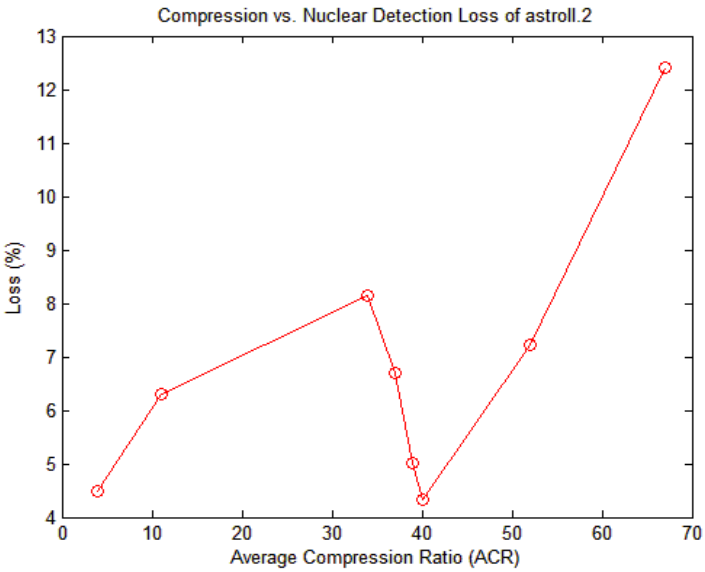

Figure 20. ACR vs. nuclear loss.

Figure 21 delineates the performances of the four types of nuclear distortion. When observing the effects of each ACR, the plot shows that the "FP" distortion type suffers the most and reaches a percentage that equals half of the raw count of nuclei. The performance of the "FN" distortion type echoes that of the plot in Figure 20. In Figure 21, the plot implies that approximately all of the detected nuclei are of the "FN" distortion

type. Hence, the nuclei are present in the raw image, but lack correspondence with nuclei in the compressed images. The "Merged" and "Split" types remain fairly stable against each ACR with percentages that hold below 2%.

Figure 22 shows the standard deviation for each of the features that belong to the morphometric group. This plot affords another way to depict the morphological response of nuclei to compression. Of the morphometric features, "Circularity" and "Extent" experience the largest deviation in error. The "Extent" feature, a function of area, is not considered a feature that helps to communicate the specificity of nuclear shapes. In terms of the five remaining features, we attribute their smaller error to the actual size of the tissue specimen in the "astroII.2" case. Our algorithm requires that an image tile possess at least 80% of tissue prior to the extraction of nuclear detail, and only 14% of "astroII.2" tiles are processed. Furthermore, the diagnosis for the "astroII.2" case does not contain a significant degree of malignancy, which also affects our algorithm's detection of astrocytes and oligodendrocytes.

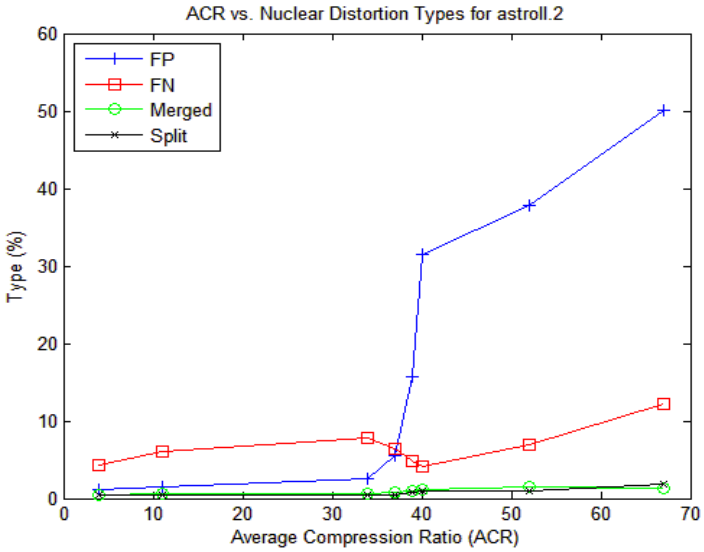

Figure 21. ACR vs. nuclear distortion types.

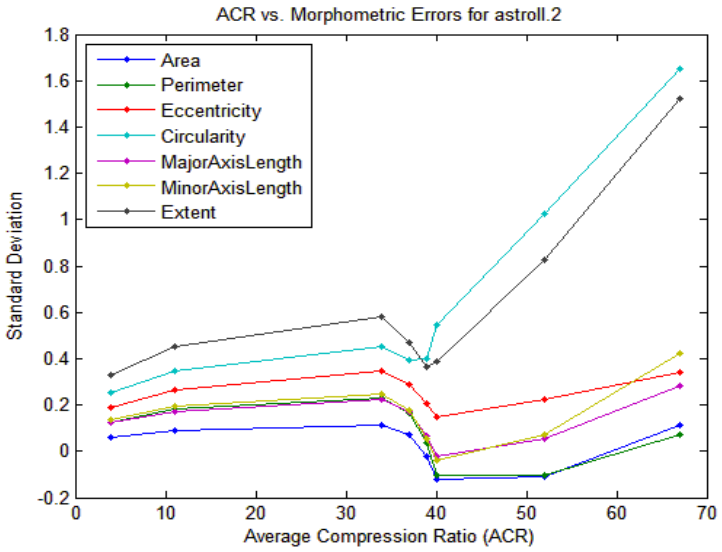

Figure 22. Standard deviation for morphometric features.

Based upon our elliptical modeling, we emphasize the features of "Circularity" and "Eccentricity" to estimate the actual changes in nuclear shape according to each ACR. Table 9 displays the quantitative results for the "Circularity" and "Eccentricity" features at the two key levels of compression. The average values of these specific features are acquired from the raw image, and the percentages indicate the number of nuclei that depart from that average value due to compression. When considering the "Circularity" and "Eccentricity" features, we observe that "Circularity" suffers the most with compression and more nuclei fall below the average by 82% at the highest ACR.

In particular, Figure 23 helps to visualize the performance of these specific features. The scatter plots show that the cluster of nuclei is more condensed for the eccentricity values approaching 1, which supports the analogy between "Idaho potatoes" and astrocytes. Table 9 and Figure 23 both demonstrate that the nuclei have significant similarity for the raw and low ACR values. Looking at the bottom plot in Figure 23, we

notice that aggressive compression clearly modifies the shape of nuclei, which increases the likelihood for tumor misclassification.

Table 9. ACR vs. Eccentricity and Circularity for astroII.2.

astroII.2			
Average Eccentricity = 0.675			
	Raw	**ACR = 11:1**	**ACR = 67:1**
≥ Average	53.78%	53.13%	61.99%
< Average	46.22%	46.87%	38.01%
Average Circularity = 0.906			
	Raw	**ACR = 11:1**	**ACR = 67:1**
≥ Average	62.70%	64.51%	17.98%
< Average	37.30%	35.49%	82.02%

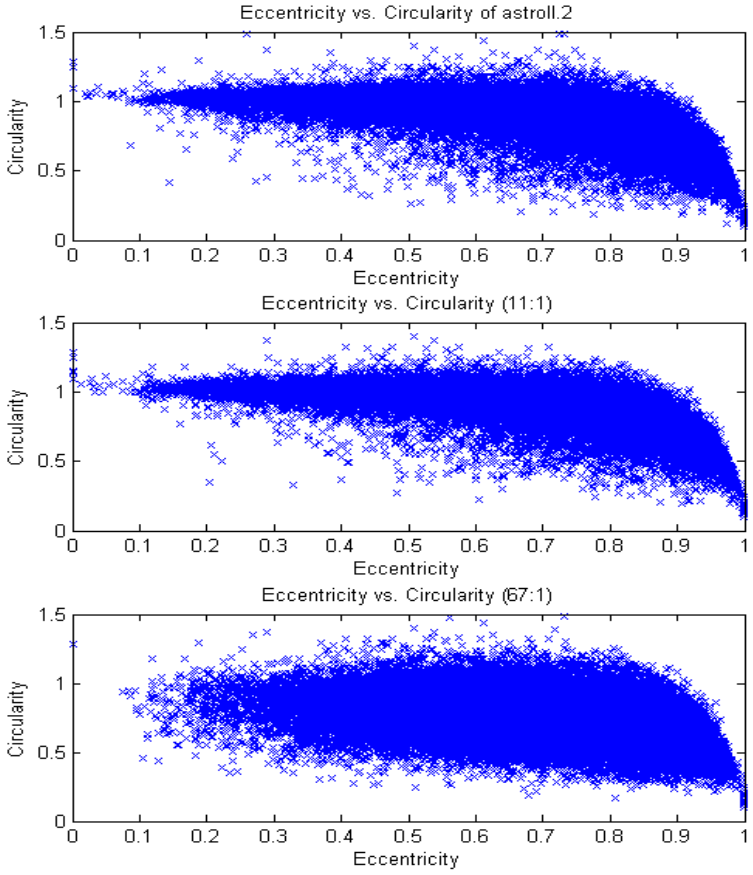

Figure 23. Eccentricity vs. circularity distribution for astroII.2.

Oligodendroglioma (Grade III): oligoIII.2

For “oligoIII.2”, the ACR range from 3:1 to 66:1. We also notice that a QF = 94 does in fact result in 10:1 compression for the “oligoIII.2” case. The raw count for the nuclei is 1,996,715 and each ACR with its associated loss of nuclei ranges from 4% to 21.6%. When comparing the nuclear detection performance at the highest compression, the percentage loss for “oligoIII.2” is almost double that of “astroII.2.” Given the significant amount of raw nuclei in “oligoIII.2”, we expect to see higher percentages in terms of degradation. The key factor is that the larger percentages of error do not compromise the relevance of the nuclear features.

According to Table 8, the misbehavior of the “FN” distortion type that is detected in “oligoIII.2” follows the same trend of that in “astroII.2.” Specifically, the “FN” distortion type and the “Loss” are within 0.5% of each other, which is negligible error in this case. While the “FN” distortion type in “oligoIII.2” carries the same implication that we see in “astroII.2”, the “FP” distortion type in “oligoIII.2” also performs in an unexpected manner. Initially, we observe that the “FP” distortion type increases to 13% at the ACR of 38:1. The “FP” distortion type then declines with even greater compression and equals 9.7% at the highest ACR of 66:1. We propose that the increase of “Merged” and “Split” nuclei is the potential source for the abrupt change in the “FP” distortion type.

With “oligoIII.2” occupying almost two million nuclei, Table 10 captures the percentages of nuclei that deviate from the raw averages for the “Eccentricity” and “Circularity” features. Table 10 also indicates that the nuclei between the raw and low ACR percentages are fairly unaffected by compression. Conversely, the highest ACR

produces a shift of 4.1% for the "Eccentricity" feature and 13.6% for the "Circularity" feature.

Table 10. ACR vs. Eccentricity and Circularity for oligoIII.2.

oligoIII.2			
Average Eccentricity = 0.732			
	Raw	**ACR = 10:1**	**ACR = 66:1**
≥ Average	56.67%	56.69%	60.79%
< Average	43.33%	43.31%	39.21%
Average Circularity = 0.842			
	Raw	**ACR = 10:1**	**ACR = 66:1**
≥ Average	57.93%	59.36%	36.76%
< Average	42.07%	40.64%	63.24%

When observing the relationship between the two features in Figure 24, we see that "oligoIII.2" is not comprised of a majority of oligodendrocytes, which would follow the "Florida orange" analogy. We expect to observe a much larger clustering of nuclei for eccentricity values that are approaching 0 to indicate that the majority of nuclei are oligodendrocytes and more circular in shape. In fact, the cluster of nuclei remains comparatively monotonous until high-level compression is applied to the image. For the ACR of 66:1, we see that the scatter plot spreads slightly towards the eccentricity value of 0 without any visible change for the values that are approaching 1. Overall, the scatter plots illustrate a well-distributed combination of oligodendrocytes and astrocytes in this case.

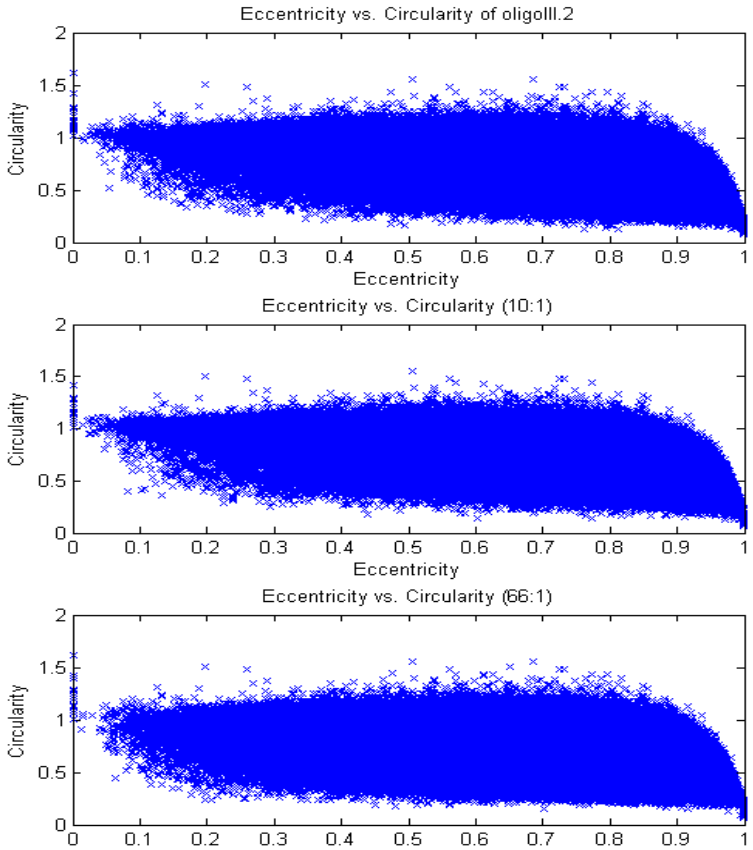

Figure 24. Eccentricity vs. circularity distribution for oligoIII.2.

Glioblastoma multiforme (Grade IV): gbm0.2

For gbm0.2, the raw count for the nuclei is 408,515 and the ACR ranges from 3:1 to 57:1. While the highest ACR for both "astroII.2" and "oligoIII.2" is approaching 70:1, the highest ACR for "gbm0.2" is only approaching 60:1. Despite the use of the same QFs, the "gbm0.2" results in 8:1 compression as opposed to the targeted 10:1. This disparity confirms the following two points: (1) The fact that we lack control over the specificity of the compression rate, and (2) The numeric relationship between the QF and the CR is not consistent across all images. The corresponding ACR with the associated loss of nuclei ranges from 3.5% to 18.3%. When comparing the information for nuclear detection, the contradictory behavior exists for each glioma WSI and at almost the same

ACR. For "gbm0.2", we see that the slope declines slightly sooner than for the "astroII.2" and "oligoIII.2" examples. As with the other examples, the plots for the detection of nuclei and the "FN" distortion type are exactly the same. Additionally, we observe that the "FP" distortion type displays abnormal behavior during the highest three levels of compression. The "FP" distortion type drops by 1%, but then immediately increases back up by 1% and terminates at 1.2%. Thus, the 1% change in nuclei is so miniscule that we consider the misbehavior in this instance as non-significant.

Table 11 delineates the percentage differences from the raw averages of the "Circularity" and "Eccentricity" features. For the "gbm0.2" case, the influence of compression on the "Eccentricity" feature is considered negligible because the difference in nuclei does not exceed 0.51% across all of the ACRs. On the contrary, the "Circularity" feature does experience a recognizable change with a percentage difference of almost 12% after the highest ACR of 57:1.

Table 11. ACR vs. Eccentricity and Circularity for gbm0.2.

gbm0.2			
Average Eccentricity = 0.762			
	Raw	**ACR = 8:1**	**ACR = 57:1**
≥ Average	57.99%	58.04%	58.50%
< Average	42.01%	41.96%	41.50%
Average Circularity = 0.774			
	Raw	**ACR = 8:1**	**ACR = 57:1**
≥ Average	54.34%	54.81%	42.94%
< Average	45.66%	45.19%	57.06%

GBM, the most aggressive anaplastic astrocytoma, is identified by high cellularity, extensive variation in structural changes of nuclei, and increased nuclear

proliferation [56]. The scatter plot in Figure 25 does not demonstrate a significant change as a result of compression. The significant presence of atypia and mitosis in a GBM tumor may increase the nuclear sensitivity to segmentation and compression. To that point, the detection of actual boundaries may be misconstrued and result in incorrect categorization of nuclear shapes. Visually, Figure 25 suggests that the nuclei in "gbm0.2" have an even distribution in shape that is quite similar to the plots of the "oligoIII.2" case in Figure 24.

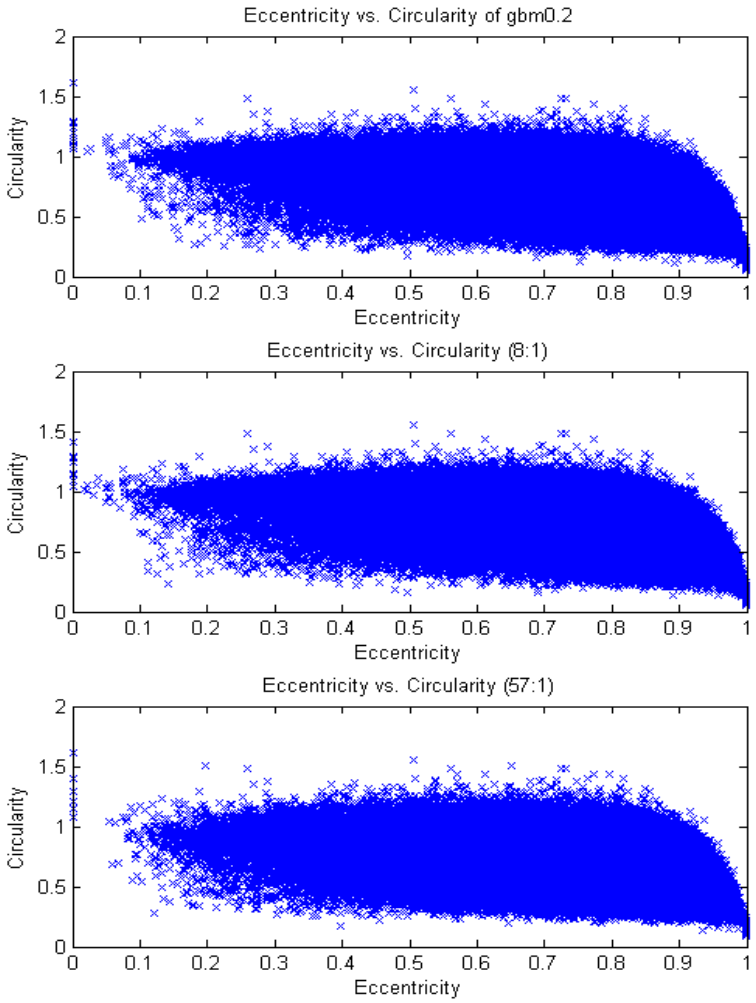

Figure 25. Eccentricity vs. circularity distribution for gbm0.2.

Summary

For each of these examples, the nuclear loss and "FN" distortion consistently display the same misbehavior. Moreover, the highly unpredicted error is seen in all 15 WSIs within our glioma-image database. We assume that the unexpected decline in the slope may be caused by the following potential sources: compression algorithm, image-content dependency, over or under segmentation, or global thresholding. The nuclear misbehavior does not appear to be a fault of image compression or to be a content-related issue. Therefore, we consider the first two possible sources as not significant contributors to the misbehavior in the nuclei.

While frequently used in many segmentation algorithms, the watershed transform can often cause over or under segmentation. The result would be that a vast number of nuclei are not properly identified during the segmentation stage. The global thresholding of nuclei that is imposed by our algorithm may be causing false or lack thereof in terms of recognition. For example, using equation 5.1 from Section 5.3.1, pertinent nuclei could be erroneously classified as background and go undetected by our algorithm. In the future, a more exhaustive study is required to provide more knowledge about the potential contributors that may affect the nuclear recognition and segmentation of a machine-based method.

In addition, we also notice that the error for each morphometric feature becomes more significant with higher compression. Despite the irregular behavior in the nuclei, the amount of nuclear distortion and morphometric error are both minimal at a level near 10:1 compression for each glioma WSI. We observe that our hypothesis regarding 10:1 compression continues to repute itself as a good metric for our DL rate. We also conclude

that our recommendation for DL is a practical criterion that benefits machine-based interpretation of digital-histopathological images as well. In summary, the ratio of 10:1 compression proves to have initial merit in support of human-based and machine-based image analysis for telepathology.

CHAPTER VI

RESEARCH BENEFITS AND FUTURE RECOMMENDATIONS

Chapter 6 entails a summary of potential benefits that result from our research on the role of image compression in telepathology and provides our recommendations for future work. The remainder of Chapter 6 is comprised of two sections. While Section 6.1 expresses several benefits of our research, Section 6.2 concludes this final chapter with recommendations for future research.

6.1 BENEFITS OF RESEARCH

The goal of this research is to enhance the pervasive use of digital images in telepathology by recommending quantitative criteria for image compression. Specifically, we promote two benefits that influence the relationship between compressed images and humans, as well as the relationship between compressed images and machines. With optimal compression, telepathology and its users can experience the following: (1) More efficient communication across capacity-constrained networks, and (2) Enhance the methods for storing large-scale images to accommodate the spectrum of digital environments in pathology.

Telepathology has received more attention in more recent years, albeit significantly behind the highly developed discipline of teleradiology. With the speed of technological advancements, the practice of pathology is witnessing a migration away from having total dependency on the traditional microscope. The work in our human-based study helps to benefit the pathologist's confidence level in regards to using

compressed images. For example, our research helps to disqualify the idea that the color complexity of pathology images cannot endure compression without affecting the diagnostically-important content.

The modeling of nuclei and extraction of morphological features with the use of a graphical user interface (GUI) was successful in developing a more user-friendly application [65]. Computerized-image analysis offers a viable solution to the traditional problems with subjectivity and reproducibility by helping to minimize the amount of manual examination. Moreover, the automation of nuclear analysis promotes a reduction in interobserver and intraobserver variability for challenging tumors. The generation of information regarding the essential features of nuclei can lead to higher concordance with the classification and grading of cancerous cells.

Although research on the effects of image compression on nuclear features is limited [66 - 67], the burden of certain resources for WSIs can be mitigated with favorable compression. The provision of such objective analysis has the potential to improve accuracy in diagnoses and prediction of clinical treatment for patients. Our machine-based study helps to confirm that sufficient compression can be applied without degrading the fidelity of the nuclear detection or quantitative analysis.

Throughout the duration of this research, several other potential benefits to the pathology community have been recognized and include the following:

- Enhance TAT of intraoperative consultations with enhanced transmission and management of digital images.
- Enable access to remote pathologists with subspecialty expertise by general pathologists of smaller communities.

- Facilitate more standardization with histopathological examinations and interpretation of important nuclear features.
- Augment the patient's health record with objective results from image analysis.

6.2 FUTURE RECOMMENDATIONS

The potential to incorporate image analysis as a pathologist's assistant poses a great opportunity for further research. The continued investigation of nuclear-feature analysis will afford greater insight about the underlying characteristics of nuclei, and potentially lead to improving the pathologist's ability to distinguish cells more accurately. As the use of WSI becomes more commonplace, the integration of image compression will probably become second nature. To that end, thorough evaluation of compression effects will enable vast amounts of information sharing while preserving diagnostic fidelity for use in multiple domains of pathology. For future research, we recommend the following open areas:

- Include human-based experiments that utilize a test environment with fixed parameters to reduce the potential effects of environmental variability.
- Extend research with a larger database (i.e., tumor type) and refine selection of the nuclear features to further the understanding of compression effects on the internal characteristics of nuclei as well.
- Relate machine-based analysis of compressed images to human assessment and measure the degree of concordance. This allows compression and ensures a solution to help reduce intraobserver and interobserver variability by providing supplemental objective analysis.

- Include the extraction of other nuclear features that are non-elliptical parameters, like mitosis and atypia, for assessment of compression-related effects. This will help to distinguish the activity that is commonly seen in different grades of malignancy from compression-induced distortion of nuclei.
- Investigate a design that involves optimization of sampling and quantization of digital-histopathological images.
- Integrate the human aspects of cognition and visual acuity to help afford new developments for objective and subjective analysis of digital-histopathological images.
- Study different types of end devices (e.g., iPad) to assess the fidelity of digital-histopathological images given the integration of mobility and compression. This will help to tackle the increasingly popular use of wireless networks for remote access.

REFERENCES

[1] American Telemedicine Association (ATA), http://www.americantelemed.org, Last Accessed August 2009.

[2] Bhatti, M.I., Akhtar, P., Ali, T.J., and Muqeet, M.A., "Implications of JP2K coding standard for MRI image based on a feature of Region of Interest in Telemedicine," *International Conference on Engineering Education (ICEE)* 2007, Coimbra, Portugal.

[3] Caramella, D., "Teleradiology: state of the art in clinical environment," *European Journal of Radiology* 1996, **22**(3): 197-204

[4] Digital Imaging and Communications in Medicine (DICOM), http://dicom.nema.org, Last Accessed November 2008.

[5] Thrall, J.H., "Part I. History and Clinical Applications," *Radiology* 2007, **243**(3): 613-7.

[6] Thrall, J.H., "Part II. Limitations, Risks, and Opportunities," *Radiology* 2007, **244**(2): 325-8.

[7] Weinstein, R.S., "Innovations in medical imaging and virtual microscopy," *Human Pathology* 2005, **36**: 317-9.

[8] Weinstein, R.S., Descour, M.R., Liang, C., Bhattacharyya, A.K., et al., "Telepathology Overview: From Concept to Implementation," *Human Pathology* 2001, **32**(12): 1283-99.

[9] Weinberg, D.S., "How is telepathology being used to improve patient care?", *Clinical Chemistry* 1996, **42**(5): 831-5.

[10] Digital Imaging and Communications in Medicine (DICOM), *Supplement 145: Whole Slide Microscopic Image IOD and SOP Classes,* ftp://medical.nema .org/MEDICAL/Dicom/Final/sup145_ft.pdf, Last Accessed August 2010.

[11] "Pathology," *Wikipedia, The Free Encyclopedia*, http://en.wikipedia.org/wiki/ Pathology, Last Accessed October 2007.

[12] Novis, D.A, and Zarbo, R.J, "Interinstitutional comparison of frozen section turnaround time. A College of American Pathologists Q-Probes study of 32,868 frozen sections in 700 hospitals," *Archives of Pathology and Laboratory Medicine* 1997, **121**(6): 559-67.

[13] Weinstein, R.S., "Telepathology Comes of Age in Norway," *Human Pathology* 1991, **22**(6): 511-3.

[14] Weinstein, R.S., "Prospects for Telepathology," *Human Pathology* 1986, **17**(5): 433-4.

[15] Leong, F.J. W-M, Graham, A.K., Gahm, T., and McGee, J.O'D.," Telepathology: Clinical utility and methodology", *Recent Advances in Histopathology 18* 1999, p. 217-40.

[16] Weinstein, R.S., Graham, A.R., Richter, L.C., Barker, G.P., et al., "Overview of telepathology, virtual microscopy, and whole slide imaging: prospects for the future", *Human Pathology* 2009, **40**(8): 1057-69.

[17] Nordrum, I., Bjorn, E., Rinde, E., Finseth, A., et al., "Remote Frozen Section Service: A Telepathology Project in Northern Norway," *Human Pathology* 1991, **22**(6): 514-8.

[18] Keogh, C., "Telepathology in the twenty-first century," *The Biomedical Scientist* 2005, p. 952-4.

[19] Williams, S., Henricks, W.H., Becich, M.J., Toscano, M., and Carter, A.B., "Telepathology for Patient Care: What Am I Getting Myself Into?", *Advances in Anatomic Pathology* 2010, **17**(2): 130-49.

[20] Dunn, B.E., Almagro, U.A., Choi, H., Sheth, N.K., et al., "Dynamic-robotic telepathology: Department of Veterans Affairs feasibility study," *Human Pathology* 1997, **28**(1): 8-12.

[21] Dee, F.R., Lehman, J.M., Consoer, D., Leaven, T., and Cohen, M.B., "Implementation of Virtual Microscope Slides in the Annual Pathobiology of Cancer Workshop Laboratory," *Human Pathology* 2003, **34**(5): 430-6.

[22] Fine, J.L., Grzybicki, D.M., Silowash, R., Ho, J., et al., "Evaluation of whole slide image immunohistochemistry interpretation in challenging prostate needle biopsies," *Human Pathology* 2008, **39**(4): 564-72.

[23] Wienert, S., Beil, M., Saeger, K., Hufnagl, P., and Schrader, T., "Integration and acceleration of virtual microscopy as the key to successful implementation into the routine diagnostic process," *Diagnostic Pathology* 2009, **4**: 3.

[24] Rojo, M.G., Garcia, G.B., Mateos, C.P., Garcia, J.G., et al., "Critical Comparison of 31 Commercially Available Digital Slide Systems in Pathology," *International Journal of Surgical Pathology* 2006, **14**(4): 285-305.

[25] Lee, E.S., Kim, I.S., Choi, J.S., Yeom, B.W., et al., "Practical telepathology using a digital camera and the internet," *Telemedicine Journal and e-Health* 2002, **8**(2): 159-65.

[26] Leong, F.J., "Practical applications of Internet resources for cost-effective telepathology practice," *Pathology* 2001, **33**(4): 498-503.

[27] Weinstein, R.S., Bhattacharyya, A.K., Graham, A.R., and Davis, J.R., "Telepathology: A Ten-Year Progress Report," *Human Pathology* 1997, **28**(1): 1-7.

[28] Black-Schaffer, S., and Flotte, T.J., "Current Issues in Telepathology," *Telemedicine Journal* 1995, **1**(2): 95-106.

[29] Halliday, B.E, Bhattacharyya, A.K., Graham, A.R., Davis, J.R., et al., "Diagnostic Accuracy of an International Static-Imaging Telepathology Consultation Service," *Human Pathology* 1997, **28**(1): 17-21.

[30] Weinstein, R.S., "Static Image Telepathology in Perspective," *Human Pathology* 1996, **27**(2): 99-101.

[31] Zhou, J., Hogarth, M.A., Walters, R.F., Green, R., and Nesbitt, T.S., "Hybrid System for Telepathology," *Human Pathology* 2000, **31**(7): 829-33.

[32] Wilbur, D.C, Madi, K., Colvin, R.B., Duncan, L.M., et al., "Whole-Slide Imaging Digital Pathology as a Platform for Teleconsultation: A Pilot Study Using Paired Subspecialist Correlations," *Archives of Pathology and Laboratory Medicine* 2009, **133**(12): 1949-53.

[33] Afework, A., Beynon, M.D., Bustamante, F., Cho, S., et al., "Digital Dynamic Telepathology – the Virtual Microscope," *Proceedings of the AMIA Symposium* 1998, p. 912-6.

[34] Barr, M., McClellan, S., Winokur, T., and Vaughn, G., "An Automated Tissue Preclassification Approach for Telepathology: Implementation and Performance Analysis," *IEEE Transactions on Information Technology in Biomedicine* 2004, **8**(2): 97-102.

[35] Dunn, B.E., Choi, H., Almagro, U.A., Recla, D.L., et al., "Telepathology Networking in VISN-12 of the Veterans Health Administration," *Telemedicine Journal and e-Health* 2000, **6**(3): 349-54.

[36] Dunn, B.E., Almagro, U.A., Choi, H., Recla, D.L., et al., "Use of telepathology for routine surgical pathology review in a test bed in the Department of Veterans Affairs," *Telemedicine Journal* 1997, **3**(1): 1-10.

[37] Dunn, B.E., Choi, H., Almagro, U.A., Recla, D.L., et al., "Routine Surgical Telepathology in the Department of Veterans Affairs: Experience-Related Improvements in Pathologist Performance in 2200 Cases," *Telemedicine Journal* 1999, **5**(4): 323-37.

[38] Guzman, M., and Judkins, A.R., "Digital Pathology: A Tool for 21st Century Neuropathology," *Brain Pathology* 2009, **19**(2): 305-16.

[39] Ferreira, R., Moon, B., Humphries, J., Sussman, A., et al., "The Virtual Microscope," *Proceedings of the AMIA Annual Fall Symposium* 1997, p. 449-53.

[40] Krupinski, E.A., Tillack, A.A., Richter, L., Henderson, J.T., et al., "Eye-movement study and human performance using telepathology virtual slides. Implications for medical education and differences with experience," *Human Pathology* 2006, **37**(12): 1543-56.

[41] Johnson, J.P., Krupinski, E.A., Yan, M., Roehrig, H., et al., "Using a Visual Discrimination Model for the Detection of Compression Artifacts in Virtual Pathology Images," *IEEE Transactions on Medical Imaging* 2011, **30**(2): 306-14.

[42] Winokur, T.S., McClellan, S., Siegal, G.P., Reddy, V., et al., "An Initial Trial of a Prototype Telepathology System Featuring Static Imaging With Discrete Control of the Remote Microscope," *American Journal of Clinical Pathology* 1998, **110**(1): 43-9.

[43] Pappas, T.N., Safranek, R.J., and Chen, J., "Perceptual Criteria for Image Quality Evaluation," *Handbook of Image and Video Processing* 2005, Academic Press, p. 939-59.

[44] Jayant, N., Johnston, J., and Safranek, R., "Signal Compression Based on Models of Human Perception," *Proceedings of the IEEE* 1993, **81**(10): 1385-1422.

[45] Foran, D.J., Meer, P.P., Papathomas, T., and Marsic, I., "Compression Guidelines for Diagnostic Telepathology," *IEEE Transactions on Information Technology in Biomedicine* 1997, **1**(1): 55-60.

[46] Cosman, P.C., Gray, R.M., and Olshen, R.A., "Evaluating Quality of Compressed Medical Images: SNR, Subjective Rating, and Diagnostic Accuracy," *Proceedings of the IEEE* 1994, **82**(6): 919-32.

[47] Marcelo, A., Fontelo, P., Farolan, M., and Cualing, H., "Effect of Image Compression on Telepathology. A Randomized Clinical Trial," *Archives of Pathology & Laboratory Medicine* 2000, **124**(11): 1653-6.

[48] Williams, S.M., Khire, S., Jayant, N., Carter, A.B., and Srinath, U., "One-Stage and Two-Stage Models for Compressing Pathology Image Slides," *Archives of Pathology & Laboratory Medicine* 2010, **134**(6): 942.

[49] Khire, S.M. (2009). *Time-sensitive communication of digital images, with applications in telepathology* (Master's thesis). Georgia Institute of Technology, Atlanta, GA. Retrieved from http://hdl.handle.net/1853/29761.

[50] Carter, A.B., Williams, S.M., and Jayant, N.S., "Diagnostically Lossless Compression of Pathology Image Slides," *Archives of Pathology & Laboratory Medicine* 2009, **133**(7): 1150.

[51] Blackboard Inc., "Blackboard at Emory University", *Blackboard Academic Suite*, https://classes.emory.edu/webapps/portal/frameset.jsp, Last Accessed April 2008.

[52] Loukas, C.G., Wilson, G.D., Vojnovic, B., and Linney, A., "An Image Analysis-Based Approach for Automated Counting of Cancer Cell Nuclei in Tissue Sections," *Cytometry Part A* 2003, **55A**(1): 30-42.

[53] Pincus, Z., and Theriot, A.S., "Comparison of quantitative methods for cell-shape analysis," *Journal of Microscopy* 2007, **227**(2): 140-56.

[54] Claes, A., Idema, A.J., Wesseling, P., "Diffuse glioma growth: a guerilla war," *Acta Neuropathologica* 2007, **114**(5): 443-58.

[55] Coons, S.W., Johnson, P.C., Scheithauer, B.W., Yates, A.J., and Pearl, S.K., "Improving Diagnostic Accuracy and Interobserver Concordance in the Classification and Grading of Primary Gliomas," *Cancer* 1997, **79**(7): 1381-93.

[56] Gupta, M., Djalilvand, A., and Brat, D.J., "Clarifying the Diffuse Gliomas: An Update on the Morphologic Features and Markers That Discriminate Oligodendroglioma From Astrocytoma," American Journal of Clinical Pathology 2005, **5**(124): 755-68.

[57] Brat, D.J., Prayson, R.A., Ryken, T.C., and Olson, J.J., "Diagnosis of malignant glioma: role of neuropathology," *Journal of Neuro-Oncology* 2008, **89**(3): 827-311.

[58] Padfield, D., Chen, Y., Roysam, B., Cline, H., et al., "Cancer Tissue Classification Using Nuclear Feature Measurements From DAPI-Stained Images*," Proceedings of 1st Workshop on Microscopic Image Analysis with Applications in Biology* 2006, p. 86-92.

[59] Hoque, A., Lippman, S.M., Boiko, I.V., Atkinson, E.N., "Quantitative Nuclear Morphometry by Image Analysis for Prediction of Recurrence of Ductal Carcinoma *in Situ* of the Breast," *Cancer Epidemiology, Biomarkers & Prevention* 2001, **10**(3): 249-59.

[60] Tarokh, A., Liu, K-Y., Zhou, X., and Wong, S.T.C., "An Iterative Approach to Nucleus Segmentation for High Content Imaging in Cancer Research," *IEEE/NLM Life Science Systems & Applications Workshop* 2006, Bethesda, MD.

[61] Thiran, J-P., and Macq, B., "Morphological Feature Extraction for the Classification of Digital Images of Cancerous Tissues," IEEE Transactions on Biomedical Engineering 1996, **43**(10): 1011-20.

[62] Boucheron, L.E., Manjunath, B.S., and Harvey, N.R., "Use of imperfectly segmented nuclei in the classification of histopathology images of breast cancer," *IEEE International Conference on Acoustics, Speech, and Signal Processing* 2010, p. 666-9.

[63] Williams, S.M., Cooper, L., Khire, S., Saltz, J.H., and Jayant, N., "Compression Effects on Computer-Based Morphological Studies," *Journal of Pathology Informatics* 2010, **1**(18): 36.

[64] Gonzalez, R.C., Woods, R.E., and Eddins, S.L. (2004). *Digital Image Processing Using MATLAB.* Pearson Education, Inc., Upper Saddle River, NJ.

[65] López, C. Lejeune, M., Escrivè, P., Bosch, R., et al., "Effects of Image Compression on Automatic Count of Immunohistochemically Stained Nuclei in Digital Images," *Journal of the American Medical Association* 2008, **15**(6): 794-8.

[66] Doyle, S., Monaco, J., Madabhushi, A., Lindholm, S. et al., "Evaluation of effects of JPEG2000 compression on a computer-aided detection system for prostate cancer on digitized histopathology,' *IEEE International Symposium on Biomedical Imaging: From Nano to Macro* 2010, p. 1313-16.

[67] Kothari, S., Chaudry, Q., and Wang, M.D., "Extraction of informative cell features by segmentation of densely clustered tissue images," *IEEE International Conference of the Engineering in Medicine and Biology Society* 2009, p. 6706-9.

VITA

SAUNYA M. WILLIAMS

Saunya was born in Pittsburgh, PA, and spent the majority of her childhood growing up in San Diego, CA. She attended four elementary schools, three middle schools, and three high schools without being the child of a parent in the military. Saunya is a first-generation college student and graduate. She graduated summa cum laude from North Carolina A&T State University with a B.S. in Electrical Engineering in 1999. In 2003, she earned a M.S.E. in Electrical Engineering from the University of Michigan.

Saunya is passionate about education and strives to inspire others to be leaders in academic excellence. She had acquired seven years of professional experience between Ford Motor Company and Raytheon Systems Company prior to relocating to Atlanta, GA in 2006. Five years later, almost to the exact day, she earned a Ph.D. in Electrical and Computer Engineering from Georgia Institute of Technology in 2011.

Saunya has research interests in image analysis, health informatics and using advanced telecommunications to enhance the delivery of patient care. She is a member of IEEE, Eta Kappa Nu, Tau Beta Pi, ASEE, and NSBE. She is the director of the Speechless Mime Ministry at Elizabeth Baptist Church in Atlanta, GA. In Saunya's spare time, she enjoys traveling, community service, and spending time with family and friends.